

**Technical Note 06 – Basis for Damage Rate
Prediction for Pressure Pipes**

VK Sadashiva (compiler)
M Nayyerloo AK Sherson

**GNS Science Consultancy Report 2017/188
December 2019**

DISCLAIMER

This report has been prepared by the Institute of Geological and Nuclear Sciences Limited (GNS Science) exclusively for and under contract to Opus International Consultants Ltd. Unless otherwise agreed in writing by GNS Science, GNS Science accepts no responsibility for any use of or reliance on any contents of this report by any person other than Opus International Consultants Ltd and shall not be liable to any person other than Opus International Consultants Ltd, on any ground, for any loss, damage or expense arising from such use or reliance.

Use of Data:

Date that GNS Science can use associated data: January 2020

BIBLIOGRAPHIC REFERENCE

Sadashiva VK, compiler, Nayyerloo M, Sherson AK. 2019. Seismic performance of underground water pipes during the Canterbury Earthquake Sequence. Lower Hutt (NZ): GNS Science. 64 p. Consultancy Report 2017/188.

CONTENTS

ABSTRACT	IV
KEYWORDS	IV
1.0 INTRODUCTION	1
2.0 CANTERBURY EARTHQUAKE SEQUENCE	2
2.1 Shaking Intensity	2
2.2 Liquefaction	4
3.0 OVERVIEW OF CHRISTCHURCH THREE WATERS NETWORKS	6
3.1 Potable Water Supply	6
3.2 Wastewater	7
3.3 Storm Water	7
4.0 PIPE DAMAGE.....	8
4.1 Network Data.....	8
4.2 Damage Data	8
4.3 Averaging of Wastewater Break Rates	11
4.4 Damage Data Screening	11
4.5 Overall Break Rates.....	12
5.0 MMI-BASED FRAGILITY FUNCTIONS.....	15
5.1 Fragility Functions Based on 'ShakeMap NZ' Intensities.....	15
5.1.1 Christchurch Break Rates	15
5.1.2 Fragility Functions	15
5.1.3 Discussion	17
5.2 Fragility Functions Based on the Dowrick and Rhoades Attenuation Model... <td>18</td>	18
5.2.1 Fragility Functions	19
5.2.2 Discussion	28
5.3 Comparison of Proposed New Fragility Models with Existing Fragility Models	28
5.3.1 The Cousins Model	28
5.3.2 Comparison with the Cousins Model.....	29
6.0 LSN-BASED FRAGILITY FUNCTIONS.....	32
6.1 Introduction.....	32
6.2 PGAs of the Canterbury Earthquake Sequence.....	32
6.3 Liquefaction Severity Number.....	33
6.4 Methodology.....	36
6.5 Correlation of Pipe Damage with LSN	36
6.5.1 Screening Criteria.....	37
6.5.2 Combing Data into Broader LSN Bands	37
6.5.3 Separating Lateral Spreading Damage	38
6.5.4 Extrapolation of the LSN Maps.....	38
6.5.5 Final Break Rates	43

7.0 CONCLUSIONS	51
8.0 ACKNOWLEDGMENTS	52
9.0 REFERENCES	52

FIGURES

Figure 2.1	ShakeMapNZ MMI maps from the 22 nd February 2011 and 13 th June 2011 earthquakes.....	3
Figure 2.2	Observed liquefaction severity maps from Tonkin & Taylor Ltd for the February and June earthquakes.....	5
Figure 4.1	Cumulative repairs to the network, showing the rate at which each system was repaired.....	10
Figure 5.1	Christchurch water and wastewater pipe break rates for different combinations of pipe material type and size, calculated for different shaking intensity levels and ground liquefaction susceptibilities	16
Figure 5.2	Isoseismals created for the February 2011 Mw 6.3 Earthquake using the D&R attenuation model.....	19
Figure 5.3	Break rates for asbestos cement water supply pipes plotted against MM intensity, derived using the D&R attenuation model, for the February and June earthquakes.....	20
Figure 5.4	Break rates for cast iron water supply pipes plotted against MM intensity, derived using the D&R attenuation model, for the February earthquake.....	20
Figure 5.5	Break rates for high-density polyethylene (HDPE) water supply pipes plotted against MM intensity, derived using the D&R attenuation model, for the February and June earthquakes.....	21
Figure 5.6	Break rates for galvanised iron water supply pipes plotted against MM intensity derived using the D&R attenuation model, for the February and June earthquakes.....	21
Figure 5.7	Ductile mains break rates.....	23
Figure 5.8	Non-ductile mains break rates.....	23
Figure 5.9	Ductile sub-mains break rates.....	24
Figure 5.10	Galvanised iron potable water sub-mains break rates.....	24
Figure 5.11	Mean break rate curve for non-ductile mains in areas where little or no liquefaction was observed.....	25
Figure 5.12	Mean break rate curve for ductile sub-mains in areas where little or no liquefaction was observed.....	25
Figure 5.13	Mean break rate curve for galvanised iron sub-mains in areas where little or no liquefaction was observed.....	26
Figure 5.14	Proposed fragility curve for ductile mains in areas with little or no observed liquefaction.....	27
Figure 5.15	Comparison of the proposed models for ductile mains with the equivalent Cousins models.....	30
Figure 5.16	Comparison of the proposed models for non-ductile mains with the equivalent Cousins models.	31
Figure 6.1	ShakeMapNZ produced PGA map of the February 22 nd 2011 earthquake.	32
Figure 6.2	ShakeMapNZ produced PGA map of the June 13 th 2011 earthquake.....	33
Figure 6.3	Smoothed LSN map of Christchurch City for the February Mw 6.2 earthquake.	34
Figure 6.4	Smoothed LSN map of the February Mw 6.2 earthquake, showing only the eastern suburbs in Christchurch.	35
Figure 6.5	Smoothed LSN map of Christchurch for the June Mw 6.3 earthquake.	35
Figure 6.6	Relationship between Christchurch water supply break rates and LSN.	37

Figure 6.7	Areas surveyed for surface liquefaction manifestation following the June event but not inspected post-February earthquake	39
Figure 6.8	Sensitivity of LSN to magnitude-weighted PGA for Christchurch residential Red Zone (major damage), TC3 (moderate liquefaction damage) and TC2 (minor damage).....	40
Figure 6.9	Christchurch water supply pipes in the 'Low', 'Medium' and 'High' LSN ranges in the February event.....	42
Figure 6.10	Christchurch water supply pipes in the 'Low', 'Medium' and 'High' LSN ranges in the June event	42
Figure 6.11	Break rates for ductile mains, comparing the damage due to the February 2011 earthquake with the June 2011 earthquake damage.....	44
Figure 6.12	Break rates for non-ductile mains, comparing the damage due to the February 2011 earthquake with the June 2011 earthquake damage	45
Figure 6.13	Break rates for ductile sub-mains, comparing the damage due to the February 2011 earthquake with the June 2011 earthquake damage	46
Figure 6.14	Break rates for galvanised iron sub-mains, comparing the damage due to the February 2011 earthquake with the June 2011 earthquake damage.....	47

TABLES

Table 3.1	Potable water pipe network data.	6
Table 4.1	Comparing break rates for potable water pipes in liquefied and non-liquefied areas.	13
Table 4.2	Comparing wastewater pipes break rates for the combined and averaged data (from both February and June earthquakes).	14
Table 5.1	Parameters of the fragility models derived from Figure 5.1.	17
Table 5.2	Parameters of the proposed new fragility curves derived using the D&R model to estimate shaking intensities for the Christchurch earthquakes	27
Table 5.3	Relative fragility factors in the Cousins model.	29
Table 6.1	Relationship of Tonkin & Taylor Ltd observed liquefaction categories with LSN classes for the unaltered part of the February and June LSN maps.....	40
Table 6.2	Relationship of Tonkin & Taylor Ltd observed liquefaction categories for the June event with LSN classes assumed for the extended part of the February LSN map.	41
Table 6.3	Break rates for ductile and non-ductile mains, ductile sub-mains and galvanised sub-mains in Christchurch for the February and June events,.....	48
Table 6.4	Break rates for ductile and non-ductile mains, ductile sub-mains and galvanised iron sub-mains in Christchurch for the February and June events,.....	48
Table 6.5	Break rates for ductile and non-ductile mains, ductile sub-mains and galvanised iron sub-mains in Christchurch for the February and June events,.....	48
Table 6.6	Ratio of break rates calculated for broad LSN ranges based on the original LSN maps (Table 6.3) over the break rates calculated using the extended LSN maps (Table 6.5).	48

APPENDICES

APPENDIX 1	MODIFIED MERCALLI SEISMIC INTENSITY SCALE FOR NEW ZEALAND	57
-------------------	--	----

ABSTRACT

The Canterbury Earthquake Sequence (from year 2010) revealed new information about how underground water pipes behave during an earthquake, especially under the influence of liquefaction. This report presents the results from studies on how the potable water, wastewater and storm water networks in Christchurch performed during the earthquakes.

Due to the vast amount of data that the Canterbury earthquake sequence has provided, new pipe fragility models were able to be formulated. Difficulties that arose from the complex sequence of earthquakes will be discussed, focusing on the way the pipes behaved during the February and June 2011 earthquakes and the contrasting effects that the two earthquakes had on the city of Christchurch.

How the network was repaired over time, including differences between the three networks and their repair priorities, and how this information was used to determine pipe damage will be discussed.

Finally, methodologies of deriving the pipe fragility models and the necessary hazard data and their effect on the proposed fragility models will be explained.

KEYWORDS

Underground pipes, earthquake, liquefaction, pipe fragility, Modified Mercalli Intensity, liquefaction susceptibility level, Liquefaction Severity Number (LSN), Canterbury Earthquake Sequence (CES).

1.0 INTRODUCTION

The 2010–2016 Canterbury Earthquake Sequence (CES) severely damaged underground potable water, storm and wastewater pipes in Christchurch, causing widespread interruptions to these services for months. Hundreds of thousands of residents were cut off from the water supply, and storm water and wastewater networks did not function after the earthquakes. Many systems were classified as being on the brink of failure (Eidinger et al. 2012). Hundreds of temporary fresh water tanks and pumps were distributed around the city, along with 10,000 portable toilets (Portaloos) and 30,000 chemical toilets to combat water shortages and to reduce the health impacts on the community.

Due to concerns about contamination of the fresh water sources and the risk of breakouts of disease and sickness, a boil water restriction was imposed for two weeks following the February 2011 earthquake. Widespread damage to the wastewater network and treatment plant led to 60 million litres of untreated wastewater getting discharged straight into multiple local water bodies and streams, with the risk of contaminating the underground aquifers (Eidinger et al. 2012). From October 2010 to February 2014, over 8,500 repairs on the water supply network and over 1,700 repairs on the wastewater network were commissioned to be completed. The storm water network was also being inspected and repaired, but at a much lower rate. A total of about 21,700 faults were discovered in the network up until March 2015, of which around 20,500 needed repair or some other attention.

In the pipe damage data from Christchurch, the storm water and wastewater repairs are classified differently to the water supply repairs. Repairs to the water supply network were based on contractors' repair notes. The contractors' notes often grouped multiple faults in one location and recorded the group as one fault. The CCTV repair process that is used to investigate storm and wastewater pipes catalogues and classifies every individual fault for assessment and/or repair. Not all repairs to the networks were economically viable, as some repairs did not sufficiently increase the functionality of the pipes to cover the cost of repair (SCIRT 2013). In the aftermath of the CES, the focus was on restoration of service rather than improving the resilience, and this required the prioritisation of repairs.

This report describes the performance of the water, wastewater and storm water networks in Christchurch during the CES, focusing on the two most damaging earthquakes in the sequence (in February and June 2011). First, a summary of the two events and the three water networks affected is given. The performance of the main pipe material types is then described through fragility models (which relates hazard intensity to damage state of asset). A description of the data and methodologies used to derive the fragility models is then provided.

Depending on availability of the required input data, two sets of fragility models have been derived that are functions of:

- Pipe class (material and size), Modified Mercalli intensity and the liquefaction susceptibility of the soil that the pipe is buried in.
- Pipe class and Liquefaction Severity Number (LSN) of the soil that the pipe is buried in.

These models can be used to simulate potential damage (or service disruption) to pipe networks in future earthquakes.

2.0 CANTERBURY EARTHQUAKE SEQUENCE

On 22nd February 2011, Christchurch City experienced a direct hit from a destructive magnitude (Mw) 6.2 aftershock following the main event of magnitude 7.1 on the 4th September 2010. The February 2011 aftershock was followed by another damage-causing aftershock of magnitude 6.4 in June 2011 and, later, by another magnitude 6.0 aftershock in December 2011. There were numerous aftershocks of smaller magnitudes in between and after these main events.

The February 2011 and June 2011 earthquakes caused severe shaking and widespread liquefaction in Christchurch. This resulted in significant physical damage to Christchurch's underground potable water, wastewater and storm water pipes. Liquefaction caused different damage modes to pipes including, but not limited to, ingress of sediments into pipes, breaks in pipes due to uneven settlement, uplift of unpressurised pipes, and joint pull-outs. The liquefaction was widespread; however, it was severe in the suburb of Bexley and along the Avon River (Cubrinovski et al. 2014).

2.1 Shaking Intensity

The shaking intensities in Modified Mercalli (MM) for the February 2011 and June 2011 earthquakes (Figure 2.1) were estimated using 'ShakeMapNZ' (a modified version of US ShakeMap for New Zealand [Horspool et al. 2015]). The MM scale is a 12-point scale in which MM1 represents barely perceptible shaking, MM6 represents the level at which damage to fragile contents of buildings begins to occur, MM7–8 represents onset of structural damage, and MM10 corresponds to significant structural damage to normal, well-designed buildings (Appendix 1). Intensities MM11 and MM12 would, in principle, result in severe damage to most construction, but this would require major deformation of the ground and the intensities have almost never been observed.

For estimating intensities, ShakeMapNZ uses model of Allen et al. (2012) that includes macro-seismic intensity data from around the globe, as well as from over 100 New Zealand earthquakes. For the February 2011 and June 2011 earthquakes, the inter-event uncertainty in the intensity prediction equation was removed by converting all observed instrumental ground motions on 25 GeoNet¹ strong motion recording stations around Christchurch into macro-seismic intensity, using the Ground Motion to Intensity Conversion Equation (GMICE) of Worden et al. (2012). More details of the methods used in ShakeMapNZ can be found in Horspool et al. (2015).

¹ www.geonet.org.nz

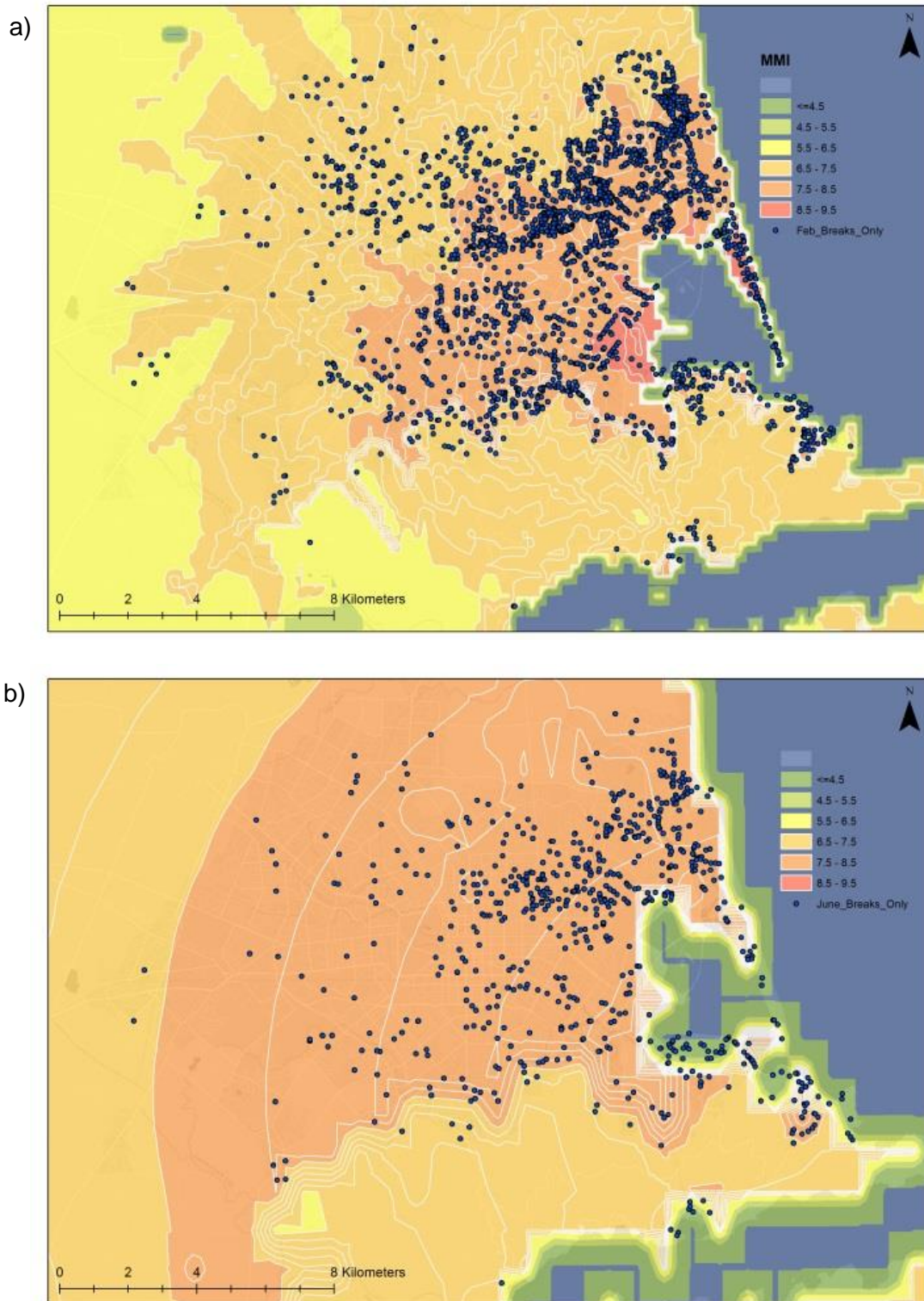


Figure 2.1 ShakeMapNZ MMI maps from a) the 22nd February 2011 and b) the 13th June 2011 earthquakes. MMI5 is the range between MM4.5 and 5.5. The dots represent faults in the potable water supply network for the respective earthquakes.

2.2 Liquefaction

Extensive liquefaction is believed to be the main cause of substantial damage to buried pipe networks in Christchurch. It is unclear how the severity of the liquefaction was impacted by increases in the confined artesian water pressure and flooding through cracks in the aquiclude (Cox 2015). One example of liquefaction damage was the uplift or floating of unpressurised pipes, such as storm water and wastewater pipes, which lead to the direction of invert changing and caused fluids to flow in undesirable directions. Rapid uplift of the pipes also caused pull-outs and shearing of joints in both pressurised and unpressurised pipes (Eidinger et al. 2012).

The liquefaction severity maps used in this study were produced by Tonkin & Taylor Ltd using information collected from drive-by surveys where evidence of liquefaction was mapped, including visible lateral spreading and sand and water ejection from the ground surface (Canterbury Geotechnical Database 2013).

Figure 2.2 shows the observed liquefaction severity maps. Liquefaction was divided into six classes, depending on the severity of the manifestation:

- **Class 0:** Not observed, presumed no liquefaction
- **Class 1:** No observed damage
- **Class 2:** Minor land damage but no observed liquefaction
- **Class 3:** Moderate liquefaction but no lateral spreading
- **Class 4:** Severe liquefaction but no lateral spreading
- **Class 5:** Moderate to major lateral spreading
- **Class 6:** Severe lateral spreading

In this report, the relationship between the severity of liquefaction and its effects on the overall break rates in Christchurch will be described. This information and its implications for producing a fragility curve will be discussed. The process will also be discussed, aiming to understand what occurred in Christchurch and the lessons we can gain from studying the performance of the Christchurch underground pipes during the CES.

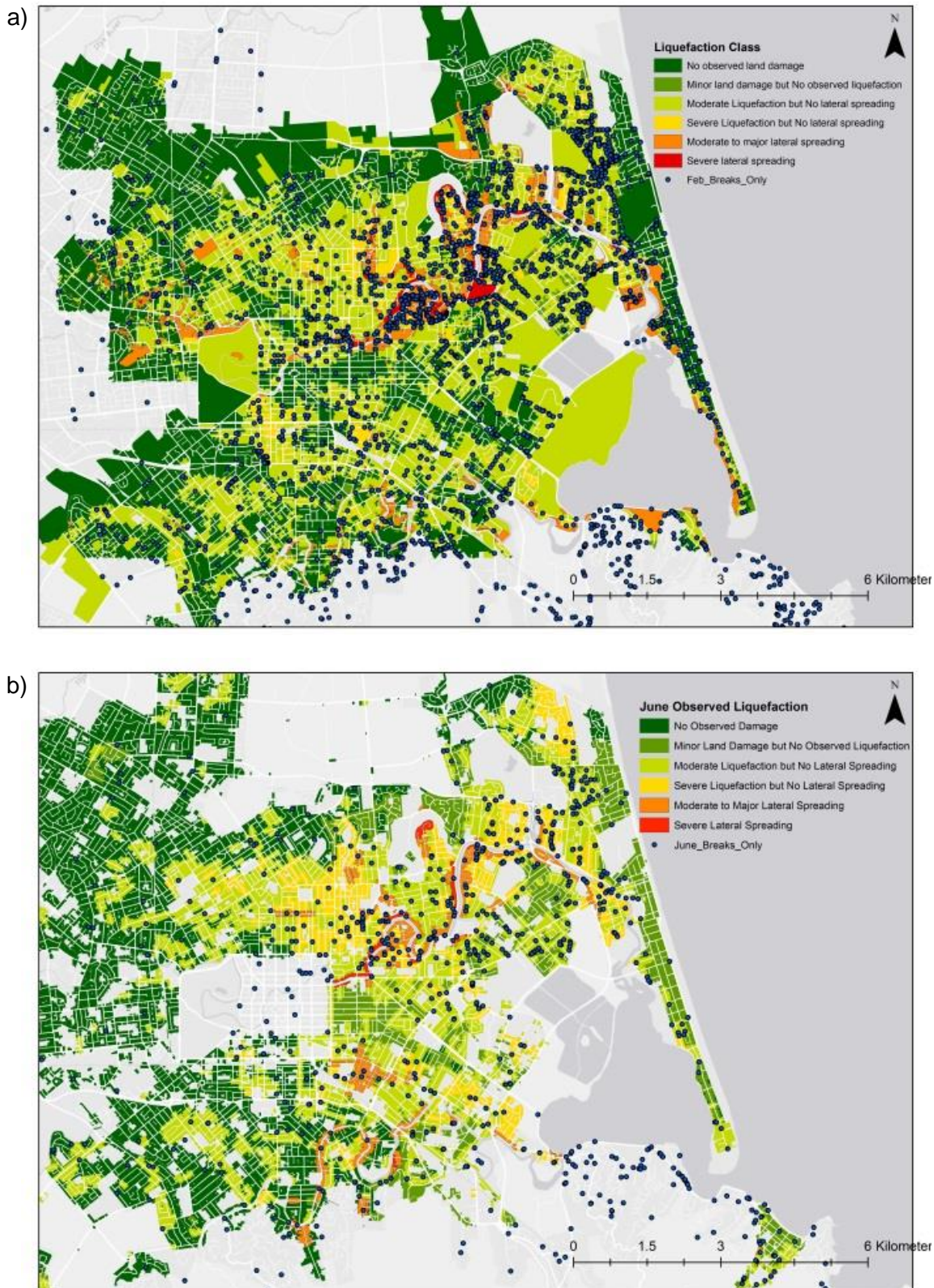


Figure 2.2 Observed liquefaction severity maps from Tonkin & Taylor Ltd for the a) February and b) June earthquakes. The dots represent pipe-breaks identified in the potable water supply networks for the respective earthquakes.

3.0 OVERVIEW OF CHRISTCHURCH THREE WATERS NETWORKS

3.1 Potable Water Supply

Christchurch City's potable water supply pipe network is made up of mains and sub-mains, each about 1,750 km long (see Table 3.1). Here, mains represent the pipes having diameters equal to or greater than 100 mm, and the pipes with diameters less than 100 mm are classified as sub-mains.

All Christchurch potable water is obtained from underground aquifers. There are approximately 150 wells at 50 different sites where water is pumped from. The water is stored in eight main reservoirs and another 37 service reservoirs (Cubrinovski et al. 2011). This network provides 100,000 cubic meters a day (100 million litres a day), totalling to about 36,525,000 cubic meters a year (36.5 billion litres a year) (Eideinger et al. 2012).

Table 3.1 Potable water pipe network data.

Pipe Type	Mains (dia. \geq 100 mm) Pipe Length		Sub-Mains (dia. < 100 mm) Pipe Length	
	km	% Length	km	% Length
Asbestos Cement (ND*) – AC	880.5	50.4	22.4	1.3
Concrete Lined Steel (D*) – CLS	56.5	3.2	0.0	0.0
Ductile Iron (D*) – DI	51.4	2.9	0.2	0.0
Cast Iron (ND*) – CI	208.5	11.9	18.7	1.1
Modified Polyvinyl Chloride (D*) – MPVC	141.7	8.1	0.6	0.0
Polyvinyl Chloride (D*) – PVC	203.2	11.6	69.2	3.9
Steel (D*) - S	49.5	2.8	1.0	0.1
Unplasticised Polyvinyl Chloride (D*) – UPVC	112.0	6.4	3.6	0.2
Galvanised Iron – GI	2.1	0.1	210.0	12.0
High Density Polyethylene (D*) – HDPE	1.0	0.1	922.2	52.6
Medium Density Polyethylene – MDPE80 (D*)	2.8	0.2	458.9	26.2
Other	36.5	2.1	46.9	2.7
TOTAL	1745.8	100.0	1753.5	100.0

* Material: Ductile (D), Non-Ductile (ND).

3.2 Wastewater

The Christchurch wastewater pipe network is around 2,000 km long. The pipes are mainly brittle materials (70%) such as concrete, asbestos cement and earthenware. The network services the entire population of Christchurch City, and has a capacity of around 6,000 litres per second (518 million litres a day) (Christchurch City Council 2013).

3.3 Storm Water

The storm water pipe network collects all rainwater and run-off from Christchurch and discharges the collected water (via. 2,000 km of underground pipes) into local rivers and streams. The pipes are mostly of brittle materials (about 70% of the network): Reinforced Concrete (RC, 54%), Concrete (CON, 5%), Earthenware (EW, 5%) and Asbestos Cement (AC, 8%). The other 30% is constructed from various other materials, which are mostly ductile.

4.0 PIPE DAMAGE

4.1 Network Data

Information on the potable water supply, wastewater and storm water networks, including the material type, age, diameter, length and location was supplied by Christchurch City Council (CCC), Stronger Christchurch Infrastructure Rebuild Team (SCIRT) and City Care Ltd. The pipe networks were segmented into 20-metre or shorter sections (section centroid represents the pipe location). This was done to ensure that each section could be assigned the characteristics of the soil that it is laid in. Each segment was then assigned a shaking intensity in MMI by geospatially joining the segment with the MMI maps. Observed liquefaction severity categories were assigned in a similar way by spatially joining the pipe segment centroid locations with the observed liquefaction severity maps from Tonkin & Taylor Ltd.

4.2 Damage Data

Pipe damage information was determined using pipe repair data which was supplied by City Care Ltd for each of the three water networks independently. Damage to water supply pipes was found to be primarily from surface observations and pressure changes. For storm and wastewater pipes, CCTV inspections were used, noting all the faults to the pipe from pipe cracks to large pipe pull-outs (SCIRT 2013).

Pipe repairs were recorded by various contractors. Repair notes included limited information about the type of repair, repair date and length of pipe repaired. Unfortunately, a lot of these data were incomplete, and different contractors used different terminologies when recording the repair processes. Consequently, there was no complete database containing accurate, comprehensive repair or replacement information. Many contractors recorded the minimum amount of information such as 'AC pipe replaced', or '3 m pipe repaired', without detailing the repair process or the material used to replace the pipe. Documenting the damage was not the contractors' highest priority in the aftermath of the CES, but valuable data was still recorded, which is used in this report to better understand the seismic performance of buried water pipes.

Inspection dates (or repair request dates) were recorded. This information is used to relate an earthquake to an observation of damage and subsequent repair. The sequence of damaging aftershocks made it difficult to determine the damage caused by a specific earthquake event. The correlation between pipe damage, shaking intensities and observed liquefaction could not always be made for an earthquake in the sequence. For example, it is not clear whether all the damage caused by an earthquake was found before the next event in the sequence or how much of the damage recorded was pre-existing before the main shock of September 2010. For water and wastewater networks, which were repaired after each event as much as was practical, the recorded inspection dates (or repair request dates) were helpful to differentiate the damage caused by each earthquake in the CES, although some assumptions had to be made.

O'Rourke et al. (2014) suggest that, as a network is restored after an event, the cumulative rate of repair (repairs per day) follows a pattern of an initial high rate of repair, followed by a transient state with an intermediate repair rate and finally a steady state of repair with a rate close to the pre-earthquake rate of repairs (i.e. 'business as usual'). The beginning of the steady state of repair shows where the repair period associated with the event ends for the water pipes in Christchurch (see Figure 4.1).

These tri-linear trends could only be established for the potable water network. For the 22nd February 2011 earthquake, the change to a steady state of repair occurs around 15th April 2011. Repairs identified in the inspection process before 15th April 2011 were considered faults/breaks directly related to the February earthquake. For the June event, the onset of transition to the steady state occurred two months after the earthquake in mid-August 2011. For the wastewater network, in the absence of clear transition points, an averaging technique was used, which will be discussed in the following section. For storm water pipes, the repairs were delayed by months until after the June event. Therefore, it was not possible to correlate the damage with any of the events to derive suitable fragility models using this method.

For each network type, each repair (relating to February and June earthquakes) was then geospatially joined with the pipe network data. The break rates or repair rates for each pipe class (combination of material type and size), liquefaction severity and shaking intensity bin were then calculated by dividing the number of repairs over the total length of pipes within the pipe class, liquefaction severity group and the intensity bin.

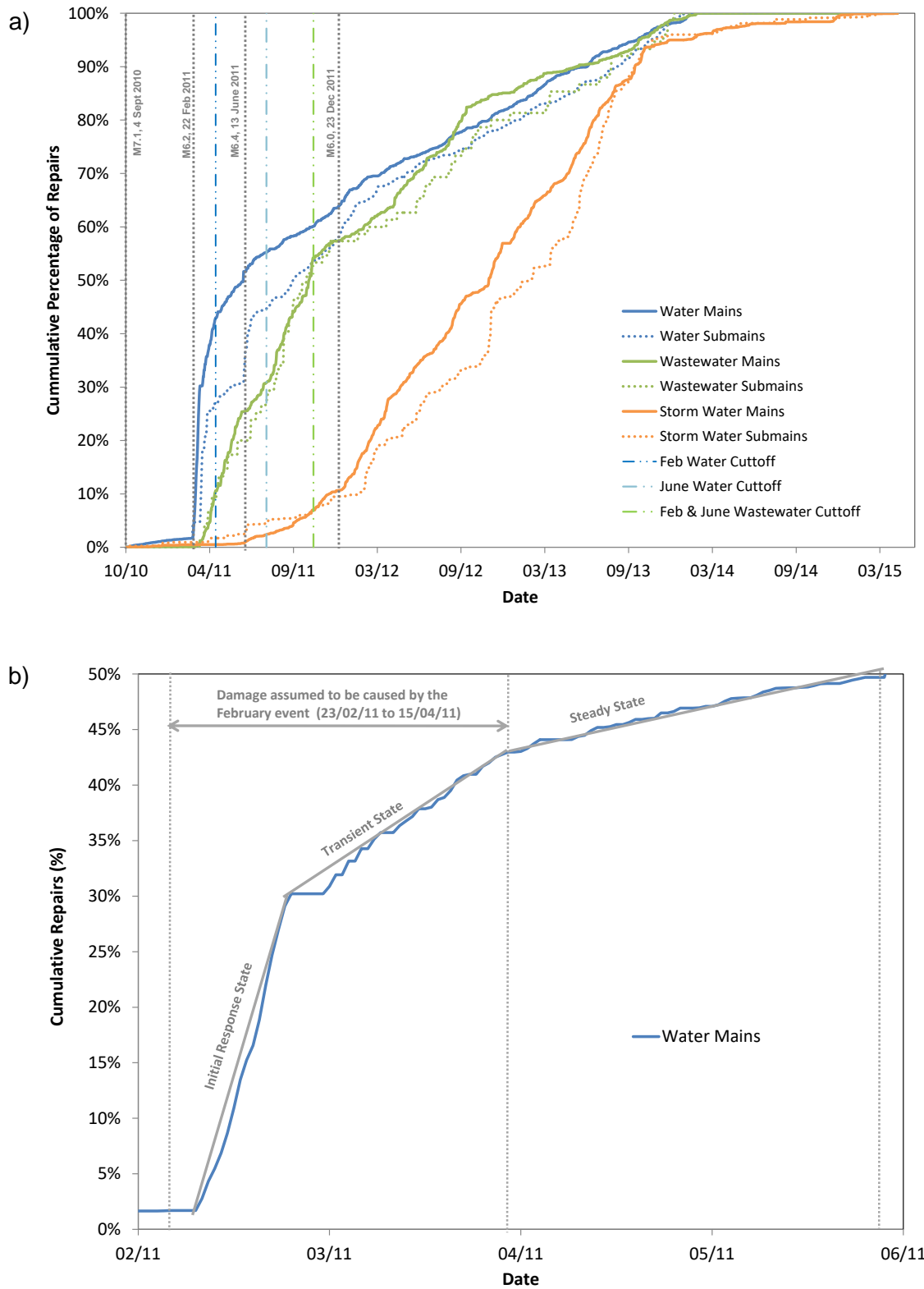


Figure 4.1 Cumulative repairs to the network, showing the rate at which each system was repaired. (a) Displays the entire repair process from October 2010 to May 2015 for all the three water networks, and (b) shows the repair process from February 2011 to June 2011 for the potable water mains only.

4.3 Averaging of Wastewater Break Rates

All repairs reported after the February earthquake and before the June event were assumed to be caused by the February event. The repairs after the June earthquake and up to the steady state of repairs (10th of November 2011) were assumed to be caused by the June earthquake. The shaking intensity and liquefaction maps from each earthquake were then used to assign the pipe fault into a shaking intensity and liquefaction severity bin for each pipe class. The average break rate for every combination of intensity and liquefaction severity was then calculated for each pipe class in every bin. This was done by summing the number of breaks in a shaking-intensity/liquefaction bin for a pipe-class and dividing the sum by the total length of pipes of the same class in the bin.

4.4 Damage Data Screening

Pipe repair rates were put through a screening process (proposed by O'Rourke and Deyoe 2004) to remove extreme break rates that arose from low sample sizes (i.e. short total lengths). The screening criterion ensures the repair rates are within 50% of the ‘true’ repair rates with 95% confidence. More details on the screening method is given below.

Assume RR is the calculated repair rate, and p is the ‘true’ repair rate or the ‘true’ probability of failure. The aim is to have a calculated repair rate that falls between $0.5p$ and $(1 + 0.5)p$, therefore:

$$0.5p \leq RR \leq (1 + 0.5)p \quad \text{Equation 4.1}$$

The ‘true’ repair rate is the probability that a single pipe segment of unit length (kilometre, metre, etc.) needs repair (success) when subjected to a given level of shaking. Since the pipe either needs a repair or does not (success or failure), the repair rate can be assumed to follow a binomial distribution, therefore:

$$\mu = np \quad \text{Equation 4.2}$$

$$\sigma = \sqrt{np(1 - p)} \quad \text{Equation 4.3}$$

Where μ is the mean, σ is the variance, and n is the number of samples (the total length) of the binomial distribution. According to the central limit theorem, when the sample size (n) is sufficiently large ($np \geq 5$ and $n(1 - p) \geq 5$) the binomial distribution can be approximated by the normal distribution; therefore, for a 95% confidence, the upper bound of Equation 4.1 can be written as:

$$1.5p = p + 1.96 \sqrt{\frac{p(1-p)}{n}} \quad \text{Equation 4.4}$$

and the lower bound as:

$$0.5p = p - 1.96 \sqrt{\frac{p(1-p)}{n}} \quad \text{Equation 4.5}$$

where 1.96 is the z-score for the confidence level chosen. Solving Equation 4.4 or 4.5 for n results in:

$$n = 15.36 \times \frac{1-p}{p} \approx 15.36 \times \frac{1-RR}{RR} \quad \text{Equation 4.6}$$

The value of n is then used to represent the minimum sample size needed for a given repair rate to be included in the mix of repair rate data to derive a suitable fragility curve. For example, the minimum acceptable length for a break rate of 0.1 per kilometre to be within 50% of the ‘true’ break rate, with 95% confidence, is 138.24 km.

The use of the above screening criterion removed all break rates that were based on total lengths less than the minimum length specified by the criterion for the break rate to be within 50% of the ‘true’ rate with 95% confidence. For the range of break rates considered in this study, the criterion of Equation 4.6 also satisfies the conditions for the normal approximation of the binomial distribution discussed above. Moreover, for larger break rates ($RR \geq 1$), the rates should be converted to per metre to get a meaningful minimum length from Equation 4.6.

4.5 Overall Break Rates

Overall break rates for the entire city pipelines are reported in Table 4.1 and Table 4.2**Error! Reference source not found.** by material type for water and wastewater networks, independently. More detailed break rates for each pipe class and different combinations of intensity and liquefaction severity are shown later in Figure 5.1. As Table 4.1 shows, the June break rates were overall lower than the February break rates for water pipes. This is, broadly speaking, consistent with the lower amount of liquefaction manifestation (Eideinger et al. 2012) and shaking experienced in the June event. The June break rates might also be affected by the fact that many weak points in the network were already damaged in the February event and most were repaired in the two months following the event, resulting in an enhanced seismic resiliency in the network. However, these pipe repairs or replacements between events are not expected to have a large effect on the total lengths reported for each material type in the table, as around less than 1% of the network was replaced with more resilient material. The break rates also show that pipes made of ductile material such as HDPE, MDPE and PVC performed a great deal better than those made of brittle material such as AC or CI. Small galvanised iron (GI) pipes were the worst performing class among the different pipe classes present in Christchurch’s three water networks. GI pipes are used mainly as laterals and therefore are very small (usually 20 or 25 mm in diameter) and have many connections. The galvanised pipes in the networks were all laid before 1980 and in some cases are around 100 years old, so possibly a lot of them are now corroded. Combination of these factors is deemed to have contributed to the very high break rates for this class of pipe. Lastly, the ratios of break rates in liquefied areas (affected by permanent ground motions) over the break rates in non-liquefied areas (affected by transient ground motions) for the studied pipe materials ranges from 2–10, demonstrating that the buried pipes are more vulnerable to permanent ground motions than to transient motions. Similar results can be drawn from the wastewater repair rates. However, these results ignore variations in the pipe sizes and shaking intensities affecting pipes within each material class.

Table 4.1 Comparing break rates for potable water pipes in liquefied and non-liquefied areas.

Eq. Event	Pipe Material	Length (km)	Length (% of Total)	Breaks (No.)	Overall Ave. BR (breaks/km)	Breaks in LAs	Breaks in NLAs	Length in LAs (km)	Length in NLAs (km)	Ave. BR in LAs (breaks/km)	Ave. BR in NLAs (breaks/km)	Ratio (LAs/NLAs)
February	HDPE	923.2	26.4%	456	0.5	286	170	337.3	585.9	0.8	0.3	2.9
	AC	902.9	25.8%	1022	1.1	732	290	236.0	666.9	3.1	0.4	7.1
	MDPE80	461.8	13.2%	98	0.2	71	27	132.8	328.9	0.5	0.1	6.5
	PVC	272.4	7.8%	78	0.3	56	22	80.9	191.5	0.7	0.1	6.0
	CI	227.1	6.5%	252	1.1	191	61	98.0	129.1	1.9	0.5	4.1
	GI	212.0	6.1%	962	4.5	649	313	88.5	123.6	7.3	2.5	2.9
	Other	499.8	14.3%	154	0.3	119	35	135.3	364.5	0.9	0.1	8.5
	TOTAL	3,499.3	-	3,022	-	2,104	918	1,108.8	2,390.4	-	-	-
June	HDPE	923.3	26.7%	126	0.1	70	56	329.9	593.4	0.2	0.1	2.2
	AC	901.8	26.1%	248	0.3	162	86	223.8	678.1	0.7	0.1	5.7
	MDPE80	465.2	13.5%	21	0.0	13	8	144.7	320.5	0.1	0.02	3.6
	PVC	271.5	7.9%	20	0.1	15	5	78.6	192.9	0.2	0.03	7.4
	CI	225.9	6.5%	71	0.3	37	34	86.2	139.6	0.4	0.2	1.8
	GI	211.9	6.1%	201	0.9	139	62	78.9	133.0	1.8	0.5	3.8
	Other	454.9	13.2%	52	0.1	41	11	121.1	333.7	0.3	0.03	10.3
	TOTAL	3,454.5	-	739	-	477	262	1,063.2	2,391.3	-	-	-

Key: Eq. = Earthquake, BR = Break Rate, LA = Liquefied Area, NLA = Non-Liquefied Area, Ave. = Average.

Table 4.2 Comparing wastewater pipes break rates for the combined and averaged data (from both February and June earthquakes).

Material	Length (km)	Length (% of Total)	Breaks (No.)	Overall Ave. BR	Breaks in LAs	Breaks in NLAs	Length in LAs (km)	Length in NLAs (km)	Ave. BR in LAs	Ave. BR in NLAs	Ratio (LAs/NLAs)
RCRR	1,366.6	33.9	356	0.26	255	101	408.3	958.3	0.62	0.11	5.9
EW	783.8	19.4	345	0.44	255	90	342.6	441.1	0.74	0.20	3.6
UPVC	722.6	17.9	39	0.05	25	14	118.9	603.7	0.21	0.02	9.1
AC	370.6	9.2	81	0.22	50	31	92.0	278.6	0.54	0.11	4.9
CONC	281.8	7.0	64	0.23	48	16	146.8	134.9	0.33	0.12	2.8
PVC	104.7	2.6	5	0.05	1	4	18.9	85.8	0.05	0.05	1.1
CI	60.1	1.5	19	0.32	14	5	29.5	30.6	0.47	0.16	2.9
HDPE	46.4	1.1	10	0.22	7	3	12.3	34.1	0.57	0.09	6.5
Other	297.0	7.4	6	0.02	5.0	1.0	96.9	200.2	0.05	0.00	10.3
TOTAL	4,033	100.0	925	-	660	265	1,266	2767	-	-	-

Key: BR = Break Rate, LA = Liquefied Area, NLA = Non-Liquefied Area, Ave. = Average.

5.0 MMI-BASED FRAGILITY FUNCTIONS

5.1 Fragility Functions Based on ‘ShakeMap NZ’ Intensities

5.1.1 Christchurch Break Rates

Figure 5.1 shows the break rate results for Christchurch water and wastewater pipe networks for the February and June 2011 earthquakes. Each point on the graph represents how a pipe (based on material type and size) performed at a given shaking intensity and a liquefied or non-liquefied ground condition.

Figure 5.1 shows break rates increasing with shaking intensity for pipes in ground classed as ‘no liquefaction’ but a more linear trend in areas where liquefaction was observed. This only applies where data (material type and size) for a pipe is available across a range of shaking intensities. For several pipe classes, the lack of data prevents similar observations being made. There are no instances where different sized pipes of the same material in ground with a similar liquefaction response were exposed to the same level of shaking. Therefore, the effect of pipe size on the seismic performance could not be evaluated using this data. However, larger pipes are generally observed to perform better during earthquakes.

5.1.2 Fragility Functions

Cousins (2013) reviewed reports of damage to water supply pipelines in eleven major earthquakes and in three published reviews (ALA 2001, 2005; Rojahn and Sharpe 1985). Cousins (2013) observed four general trends within the available data, which are all consistent with the Christchurch observations: (a) damage to pipes increases with shaking intensity, (b) damage to pipes increases when damage to ground (liquefaction or lateral spreading) occurs, (c) damage to pipes decreases with increasing pipe diameter and (d) damage to pipes depends on pipe material and jointing method.

The data that Cousins used were screened according to the criteria in Section 4.4 (shown as grey points in Figure 5.1) and combined with the Christchurch data to derive appropriate fragility models. Some data were removed during screening because there was not enough surveyed length to meet the minimum sample size required. The effect of pipe size also had to be ignored to enable the combination, and therefore the reported fragility models for each class are applicable to all pipes smaller than 300 mm. The power model of Equation 5.1 best fitted the data for most classes, with a few exceptions where the coefficient of determination (R^2) was too low (< 0.25) for the trendline to be reported:

$$BR [km^{-1}] = a \times MMI^b \quad \text{Equation 5.1}$$

Here, BR is the break rate representing number of pipe breaks per kilometre, and a and b are curve fitting constants for each pipe class shown in Table 5.1. As can be seen in the table, the R-squared (R^2) values are low for some classes. The large uncertainty implied by the low R^2 values show that changes in the break rates for some pipe classes are not well captured by increased shaking intensities.

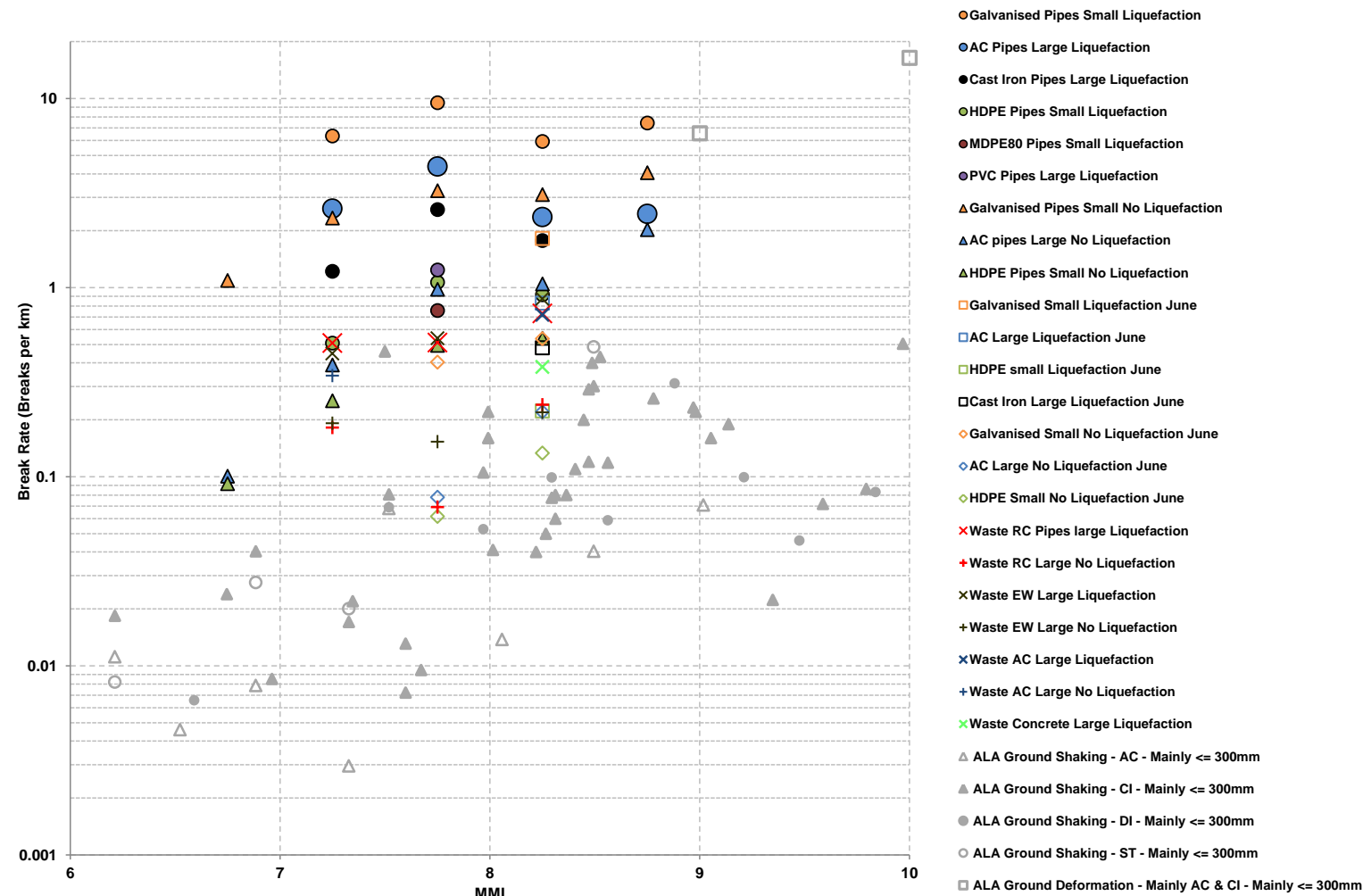


Figure 5.1 Christchurch water and wastewater pipe break rates for different combinations of pipe material type and size, calculated for different shaking intensity levels and ground liquefaction susceptibilities. Small wastewater pipes are smaller than 150 mm and small water pipes are smaller than 100 mm. (ALA 2001, 2005). AC = asbestos concrete; CI = cast iron; HDPE = high-density polyethylene; MDPE80 = medium density polyethylene with a minimum strength of 8 MPa; PVC = polyvinyl chloride; RC = reinforced concrete; EW = earthenware; DI = ductile iron; ST = steel.

Table 5.1 Parameters of the fragility models derived from Figure 5.1.

Pipe Material	Ground Condition	a	b	R ²
Asbestos Cement (AC)	Non-liquefied	5.00e-10	9.3236	0.25
	Liquefied	1.00e-05	5.8428	0.30
Cast Iron (CI)	Non-liquefied	8.00e-08	6.5747	0.33
	Liquefied	5.00e-08	8.3512	0.57
Reinforced Concrete (RC)	Liquefied	2.00e-03	2.7591	0.74
Earthenware (EW)	Liquefied	2.00e-05	5.1093	0.93
Ductile iron (DI)	Non-liquefied	6.00e-07	5.4013	0.44
Steel (ST)	Non-liquefied	6.00e-13	12.659	0.88

5.1.3 Discussion

The effect of liquefaction in Christchurch was horizontally and vertically non-uniform, with changes in severity apparent within the same mapped liquefaction severity class, particularly where the observed liquefaction was moderate or greater (Cubrinovski et al. 2014). The liquefaction maps (Cubrinovski et al. 2014; O'Rourke et al. 2014) show liquefaction severity at a scale appropriate for the map presentation, and at a site within a mapped liquefaction class the actual liquefaction may be more or less severe. However, the data clearly shows the presence of liquefaction increased the overall break rates. For example, galvanised iron pipes in areas of severe liquefaction had break rates of up to eight breaks per kilometre, which is nearly 20 times higher than the break rates observed in similar sized galvanised iron pipes in non-liquefied areas subjected to the same level of shaking.

Comparing the predicted ShakeMapNZ intensities for the February earthquake with the observed shaking intensities (GeoNet ‘Felt Reports’ and observed damage to buildings), it shows that the ShakeMapNZ intensities are about one MMI unit lower for the MMI range above 8.0 and therefore underestimate stronger shaking intensities (Goded et al. 2016; Stirling et al. 2015).

The lack of differentiation across a range of intensities when using ‘ShakeMapNZ’ required using another measure of intensity to enable better fragility models to be derived from the data. The model of Allen et al. (2012) used in ‘ShakeMapNZ’, and other similar shaking intensity prediction models, is not suitable for modelling shaking intensities over MM8 due to a lack of data to constrain the models (Goded et al. 2016). A study by Stirling et al. (2015) comparing the predicted intensities for the Christchurch earthquakes using the normal Ground Motion Intensity Conversion Equations² (GMICEs), such as the model of Allen et al. (2012) with intensities assigned based on observed damage from the public (GeoNet ‘Felt’ reports) and building survey information, shows that the GMICEs underestimate shaking intensities of MM8 and above by about one intensity unit.

² A GMICE allows conversion between measured shaking parameters, such as Peak Ground Acceleration (PGA), and predicted earthquake intensities, such as MMI.

The areas in the eastern suburbs of Christchurch with moderate or greater liquefaction damage after the February 2011 earthquake had the highest break rates in Christchurch at an MMI of 8.0 (ShakeMapNZ). However, areas further to the south with no liquefaction and higher shaking intensities (MMI of 9.0; ShakeMapNZ) had lower break rates. The data in Figure 5.1 show that break rates in areas of moderate or greater liquefaction are independent of the shaking intensity at the site whereas, in the absence of liquefaction, the pipe break rate correlates well with shaking intensity where, as the shaking intensity increases, the number of pipe breaks recorded per kilometre also increases.

The CES involving multiple large earthquakes (aftershocks) raises questions about cumulative damage across several earthquakes spaced months apart and how much damage was caused by each event. The timing of multiple earthquakes over several months during the CES may reduce the applicability of the Christchurch results to other areas for modelling risk to underground pipes from earthquakes. However, it still represents one of the most comprehensive datasets available, particularly with regards to the damage caused by liquefaction to underground pipe networks.

5.2 Fragility Functions Based on the Dowrick and Rhoades Attenuation Model

The Dowrick and Rhoades model (Dowrick and Rhoades 2005; Smith 2002) describes the attenuation of MM intensity for New Zealand earthquakes by defining shaking intensity contours called isoseismals. An ‘intensity zone’ is then the area between two adjacent isoseismals. For example, the MM5 Zone is the area between the MM5 and MM6 isoseismals. The MM shaking intensity values are constrained to be integer numbers because of the way in which the MM intensity scale is defined. They are discrete variables. In reality, the attenuation of shaking is a gradual process, and for attenuation modelling, the intensities are treated as continuous variables, i.e. they are regarded as having fractional values. The MM5 isoseismal is defined as intensity 5.0, MM6 as 6.0, and so on. The intensity at the point midway between the MM5 and MM6 isoseismals is MM5.5. The attenuation models predict the radii of continuous-variable isoseismals, rather than integer-variable ones.

The Dowrick and Rhoades (D&R) model uses the magnitude of the earthquake, location, focal depth, focal mechanism and the orientation of the fault source. The modification proposed by Smith (2002) applies to large earthquakes where the fault rupture exceeds 30 km. It extends the D&R model, where necessary, to include the full length of the fault rupture in the MM9 intensity zone. As a further modification, Smith (2002) proposed that intensities of MM10 and higher should be modelled occurring at random locations along a fault trace, i.e. not all the way along it.

The D&R model predicts shaking intensities for average ground (defined as shallow soil in NZS 1170.5). Actual intensities on non-average ground can be higher (e.g. deep or soft soil) or lower (e.g. rock) than the average-ground case. Various phenomena can be involved with the amplification of shaking by deep or soft soils of relevance to this study. Despite this limitation, the D&R attenuation model of MM shaking intensity (Dowrick and Rhoades 2005; Smith 2002) is a better match for MM shaking intensities based on observational data, particularly for MM8 or greater shaking in New Zealand.

Figure 5.2 shows the isoseismals created for the February 2011 Mw 6.3 Earthquake using the Dowrick and Rhoades model.

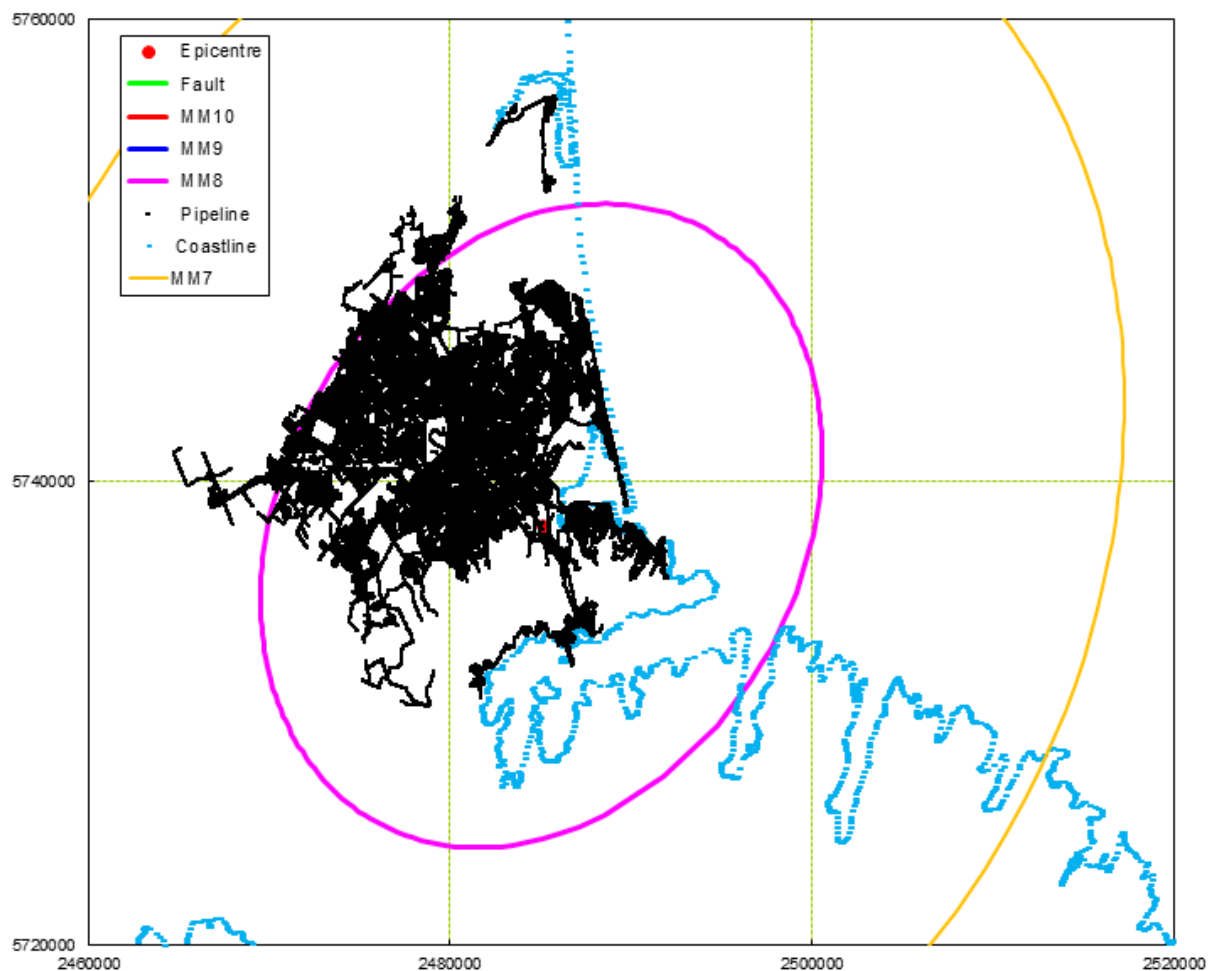


Figure 5.2 Isoseismals created for the February 2011 Mw 6.3 Earthquake using the D&R attenuation model.

5.2.1 Fragility Functions

Pipe break rates relating to the February and June earthquakes were re-calculated following the procedure described in Sections 4.1–4.3 for the MM intensities derived from the D&R attenuation model. The resulting break rates are shown in Figures 5.3–5.6. The results are separated by material type, pipe size (< 100 mm or ≥ 100 mm in diameter for sub-mains and mains, respectively) and the Tonkin & Taylor Ltd observed liquefaction class, where Classes 0, 1 and 2 are classified as ‘Low’, Class 3 as ‘Moderate/Medium’, Class 4 as ‘High’, and Classes 5 and 6 as ‘Lateral Spreading’.

It is evident in the figures that, for both events when there is liquefaction contribution to the break rates, the rates do not change much by increasing or decreasing MMI and the damage seems to be only a function of the level of liquefaction susceptibility. This is expected given that liquefaction is not adequately considered in the D&R model to estimate the intensities. This is because, in most of the events that their intensity data were used to derive the D&R model, there was no liquefaction.

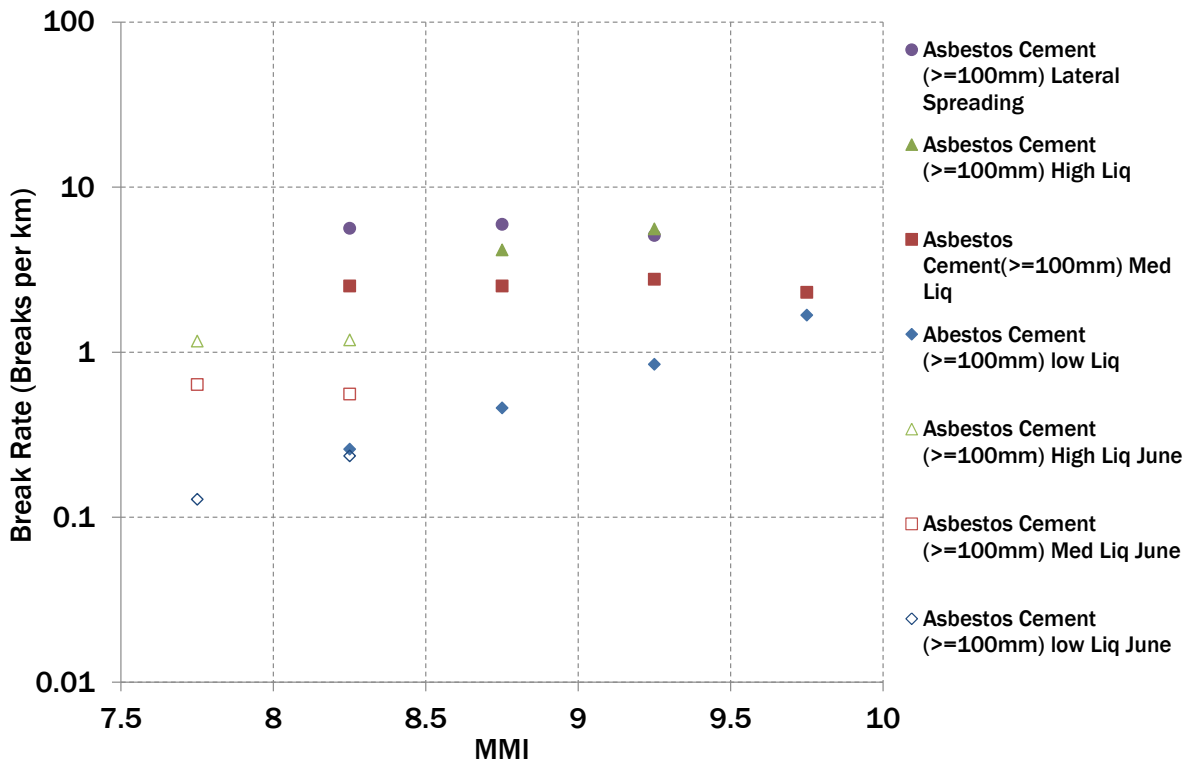


Figure 5.3 Break rates for asbestos cement water supply pipes plotted against MM intensity, derived using the D&R attenuation model, for the February and June earthquakes.

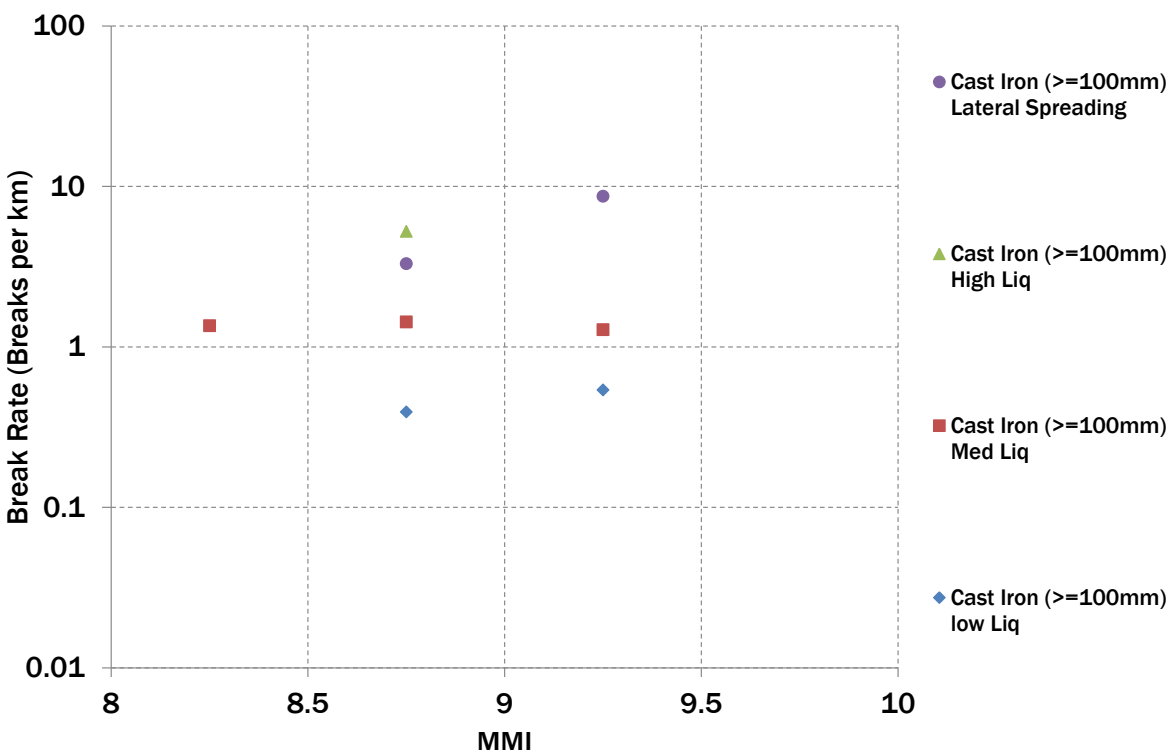


Figure 5.4 Break rates for cast iron water supply pipes plotted against MM intensity, derived using the D&R attenuation model, for the February earthquake.

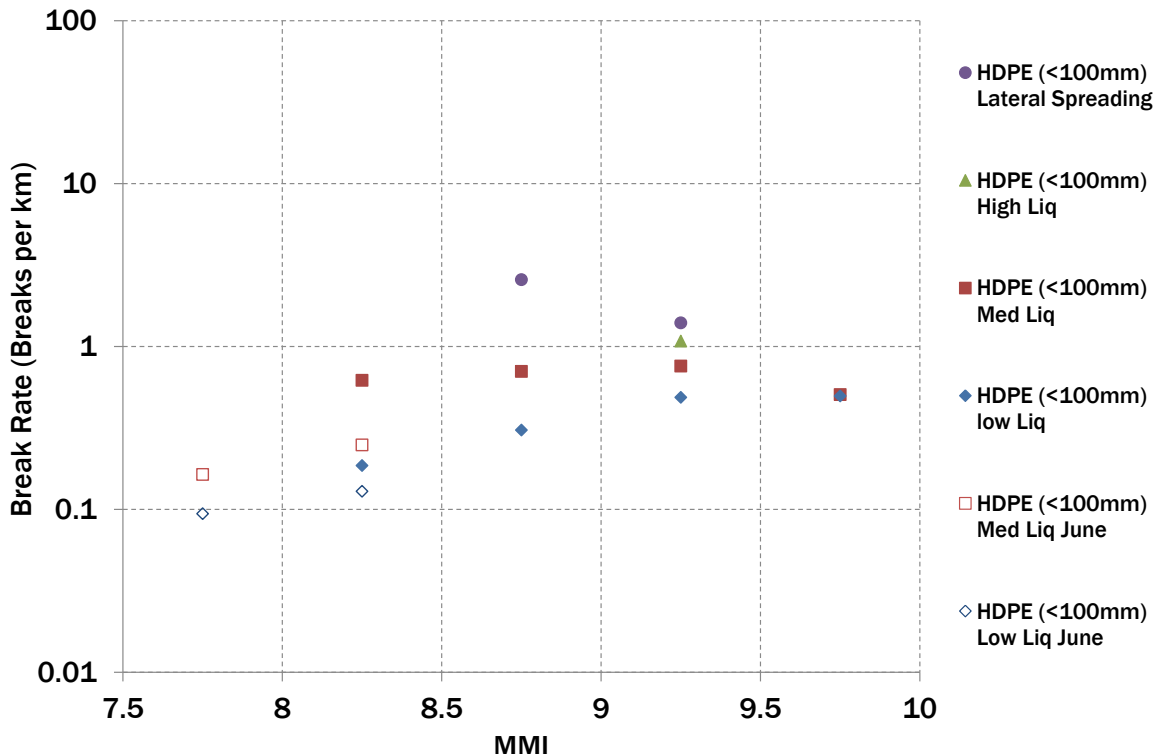


Figure 5.5 Break rates for high-density polyethylene (HDPE) water supply pipes plotted against MM intensity, derived using the D&R attenuation model, for the February and June earthquakes.

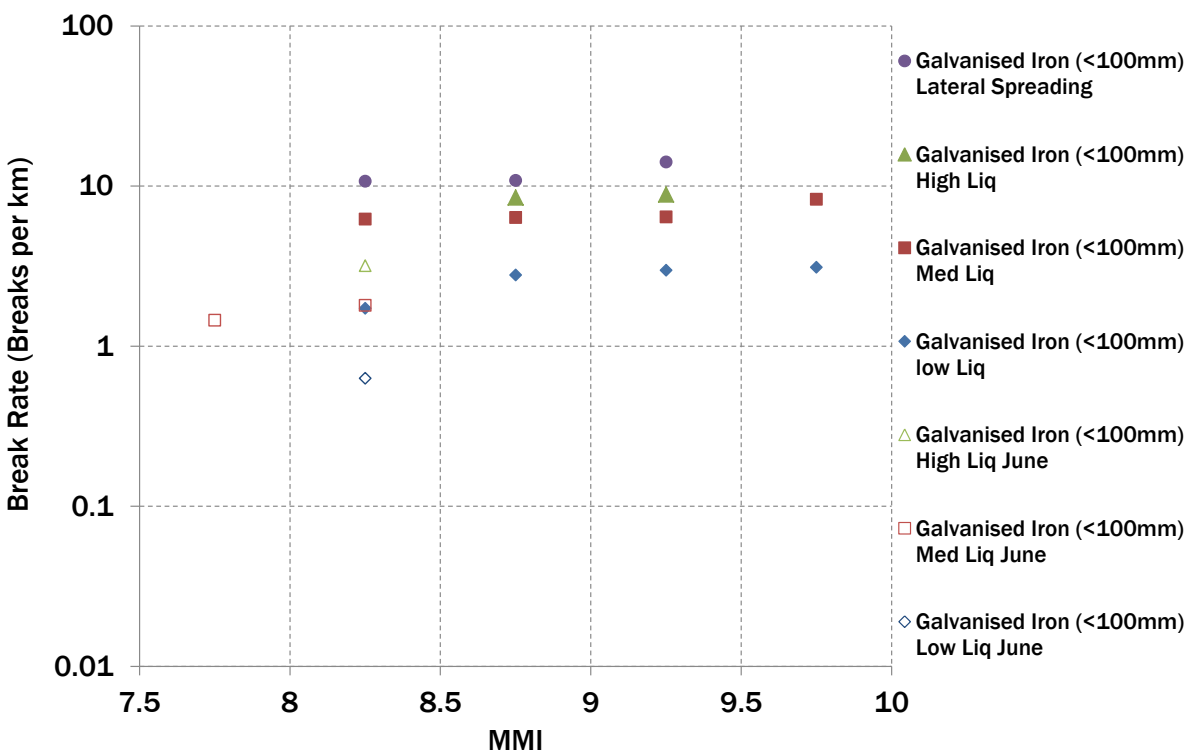


Figure 5.6 Break rates for galvanised iron water supply pipes plotted against MM intensity derived using the D&R attenuation model, for the February and June earthquakes.

The American Lifelines Association (ALA 2001) break rates were then combined with the Christchurch break rates for asbestos cement and cast iron, which were the material types in common in the two datasets. However, classes derived from a combination of material type,

pipe diameter and the pipe ground liquefaction susceptibility did not provide enough data to fit a curve to break rates. Therefore, the available data were combined into four classes defined by pipe size (< 100 mm or ≥ 100 mm in diameter) and material ductility:

- Ductile mains (DM)
- Non-ductile mains (NDM)
- Ductile sub-mains (DSM), and
- Non-ductile sub-mains (NDSM).

The non-ductile sub-mains category included mainly galvanised iron pipes and therefore was renamed accordingly. By combining the different material types into ductility classes and pipe sizes, the number of breaks rate points per class passing the screening criteria also increased and provided more data to derive a curve. The resulting break rates for the four pipe classes are shown in Figures 5.7–5.10. In the figures, the data are presented for February (filled markers), June (unfilled markers) and American Lifelines Association (crosses, plusses, stars and dashes). Each event has been screened separately and added to the plot. After combining the data into the four categories, there was insufficient data in the ductile mains category to derive a curve. However, the other three pipe classes had enough data to develop fragility models.

The wastewater pipe break rates are somewhat lower than the potable water pipe break rates, having break rates similar to the June earthquake break rates for the water supply pipes (Figure 5.8). After examination of the damage data, the wastewater break rate data was removed from the analysis for the following reasons:

- Lack of comparable data for the number of breaks present before the earthquakes, i.e. how much of the pipe damage pre-dated the earthquakes and how much was directly attributable to the CES earthquakes is unknown.
- Non-pressurised wastewater pipes behave differently compared to pressurised water pipes (Zare 2012).
- The damage issues in the wastewater pipe network were different to those found in the pressurised potable water network. This included the sensitivity of the wastewater network to changes in gradient and the intrusion of sediments into the pipes.

In areas with higher liquefaction severities (moderate liquefaction, high liquefaction or lateral spreading) the relationship between break rate and MM intensities was mostly constant across a range of MM intensities. This may indicate that, once liquefaction has occurred in an area, the extent and severity of pipe damage does not change as shaking intensity increases. This makes the threshold intensity at which damage occurs important. For areas vulnerable to liquefaction-induced ground damage, the damage can be reported as a break rate with standard deviation when MM intensities are above the threshold for liquefaction. From the data presented here, the threshold is below MM8.

A fragility curve was developed for the ‘low’ liquefaction susceptibility class (little or no liquefaction damage observed) for each pipe ductility type where there was sufficient data (i.e. non-ductile mains, ductile sub-mains and non-ductile sub-mains). A mean break rate curve was derived by calculating the mean break rates for each MM intensity. The break rates from the different earthquakes were averaged to arrive at a single mean break rate for each MM intensity. The resulting best-fit curves are shown in Figures 5.11–5.13.

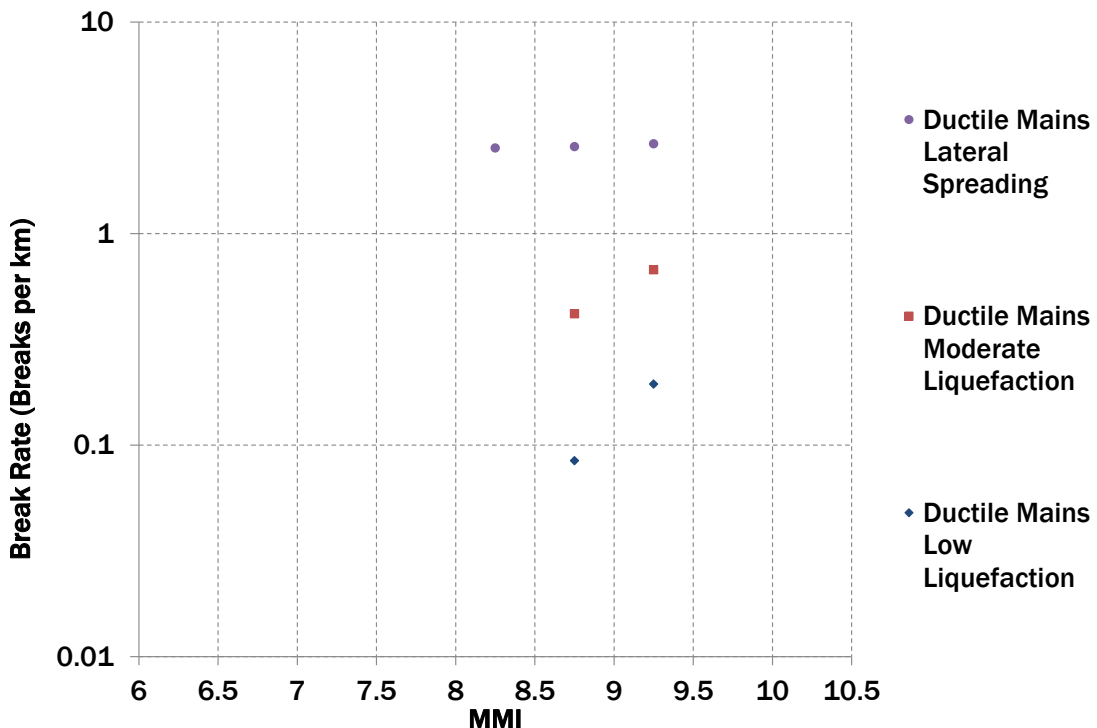


Figure 5.7 Ductile mains break rates.

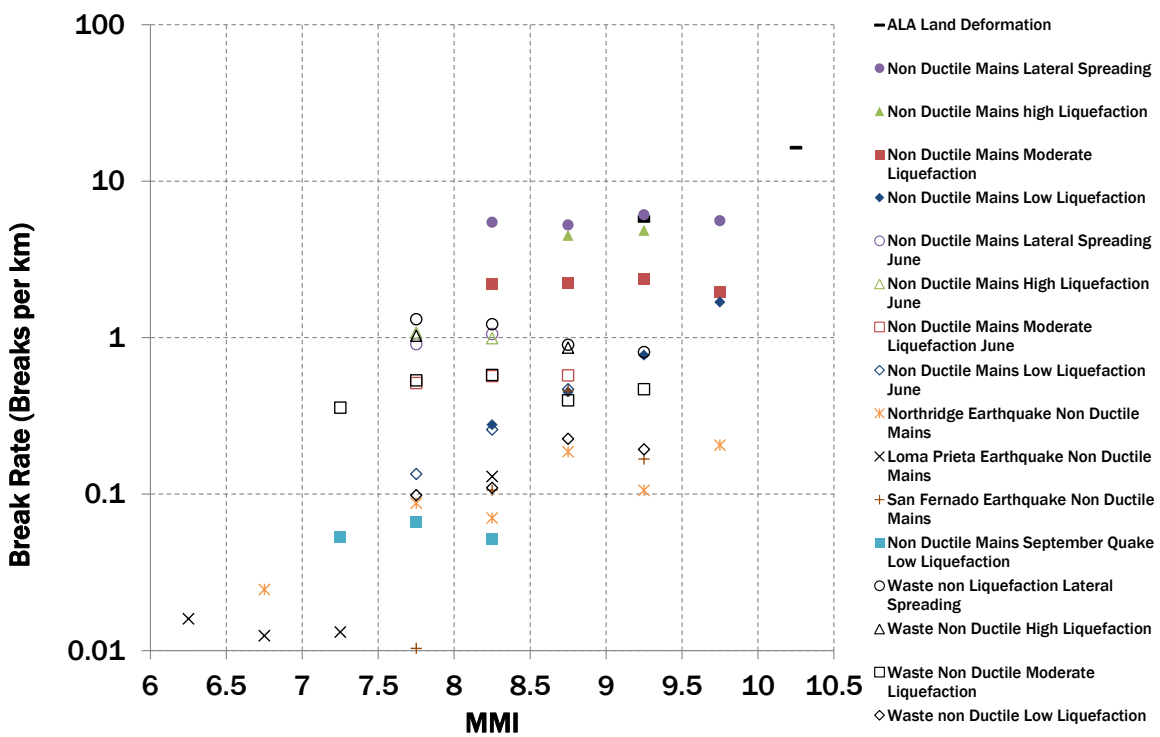


Figure 5.8 Non-ductile mains break rates.

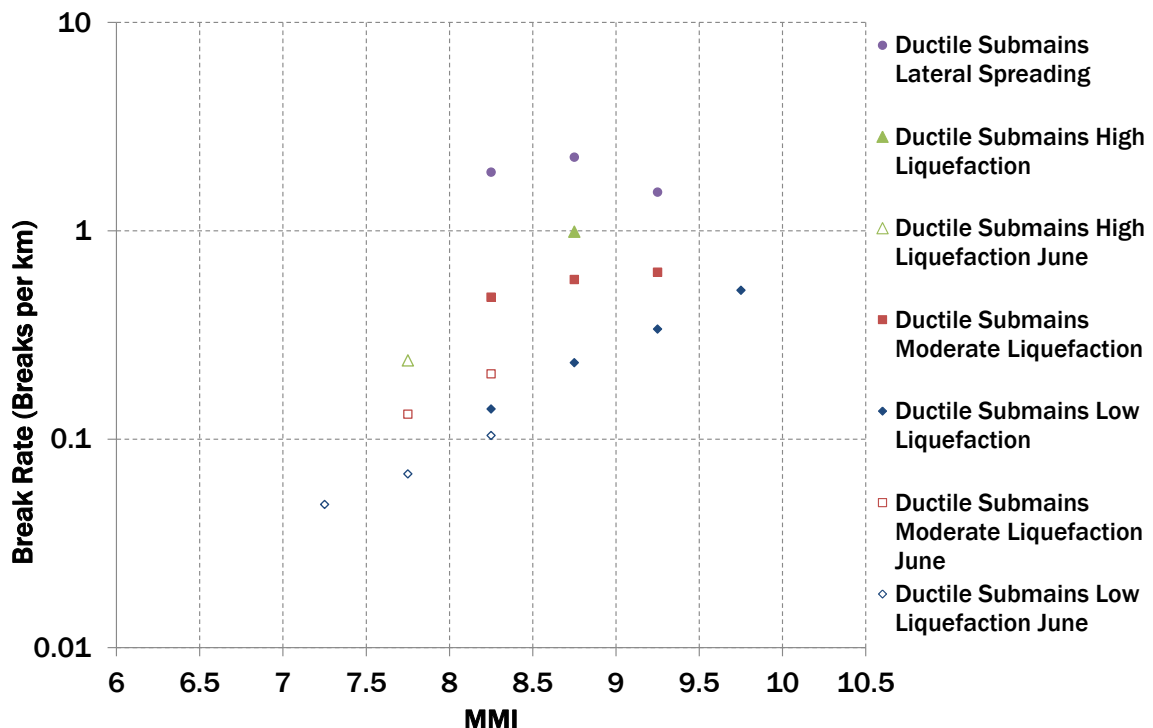


Figure 5.9 Ductile sub-mains break rates.

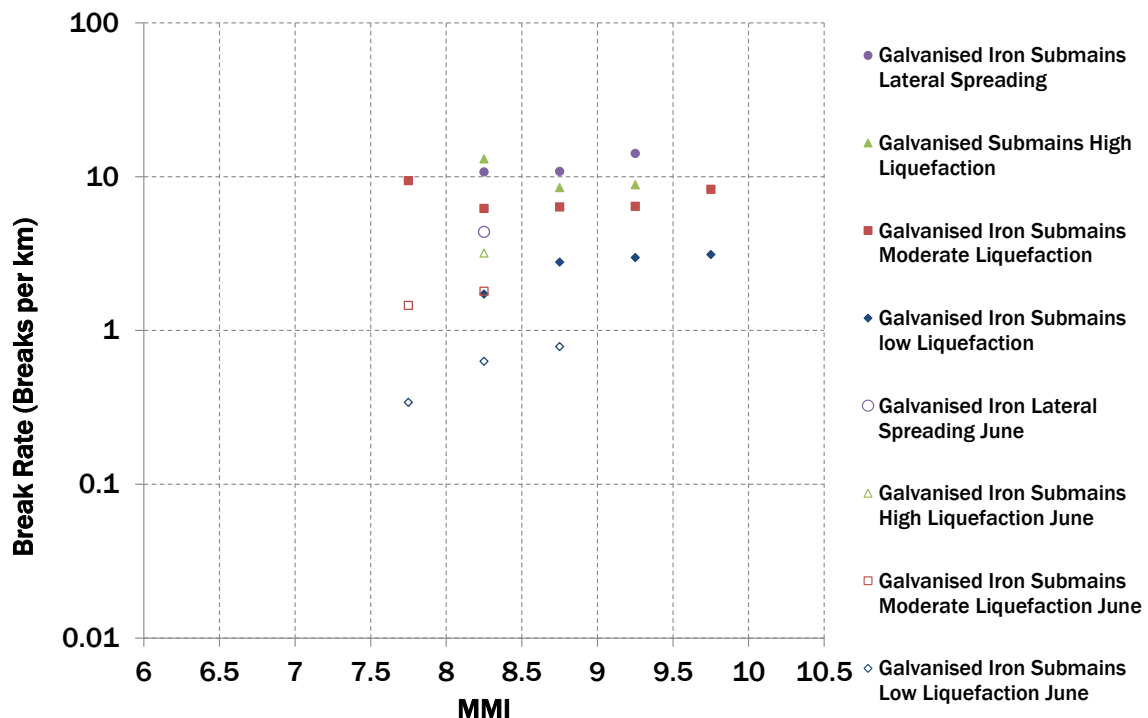


Figure 5.10 Galvanised iron potable water sub-mains break rates.

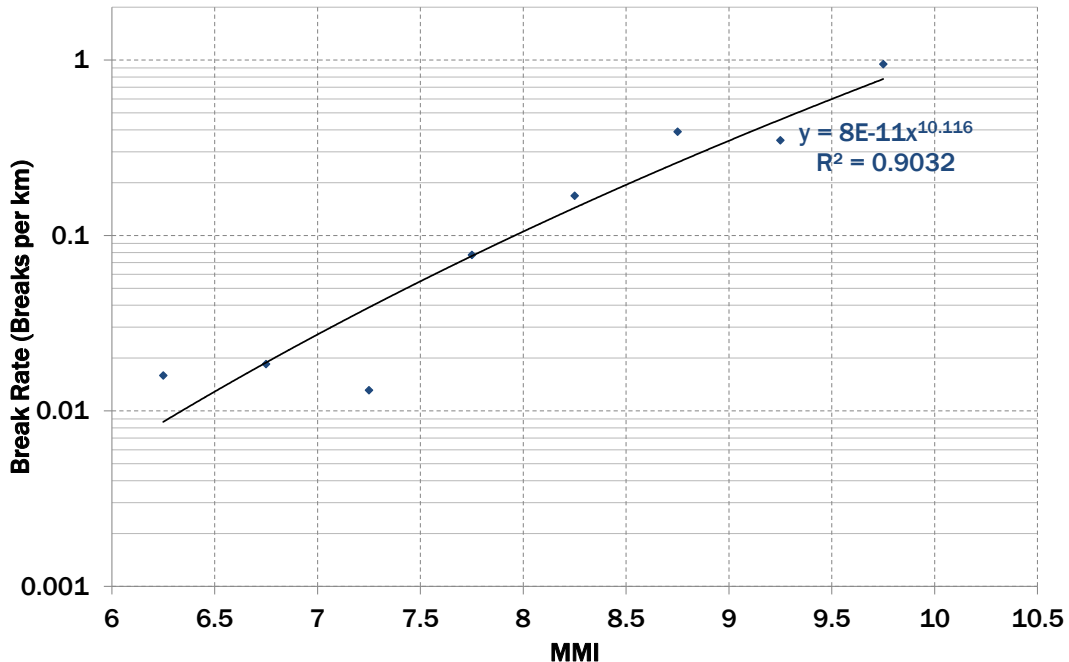


Figure 5.11 Mean break rate curve for non-ductile mains in areas where little or no liquefaction was observed.

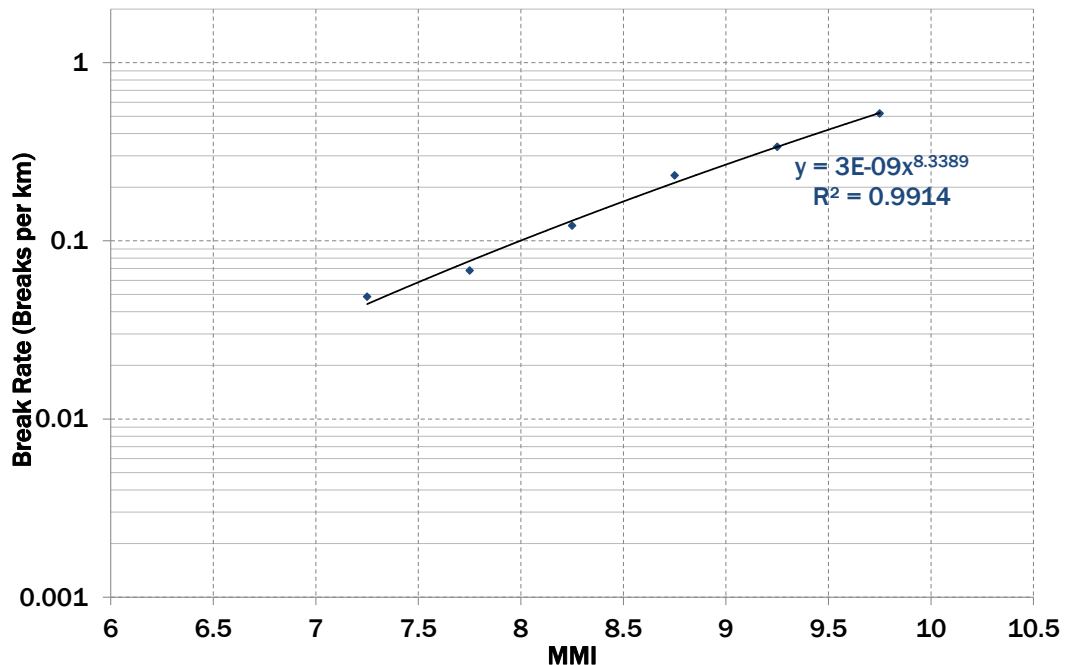


Figure 5.12 Mean break rate curve for ductile sub-mains in areas where little or no liquefaction was observed.

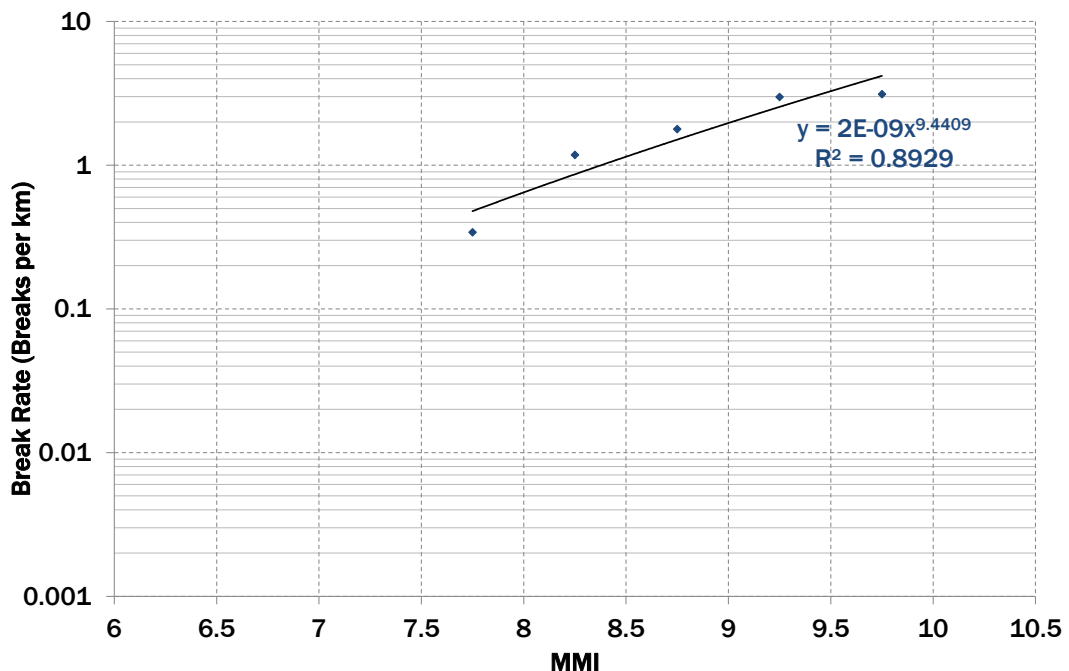


Figure 5.13 Mean break rate curve for galvanised iron sub-mains in areas where little or no liquefaction was observed.

For ductile mains, only two data points were available for break rates in areas with little or no liquefaction, so it was not possible to derive a fragility curve solely from the data. A fragility curve for ductile mains was obtained by using the best-fit curve for non-ductile mains and scaling it to pass through the means of the two ductile mains break- rates (y-axis) and the respective MM intensities (x-axis). Figure 5.14 shows these curves.

For the galvanised iron sub-mains, the break rates are much higher than expected when compared with the ductile sub-mains break rates (~5–9 times higher). This could be attributed to the age and size of the Christchurch galvanised iron pipes, which are very small, old and possibly corroded. A separate mean break rate curve is proposed for the non-ductile sub-mains class. This was done by scaling up the ductile sub-mains curve using the same scaling relationship developed for the mains category. The proposed mean break rate parameters are summarised in Table 5.2.

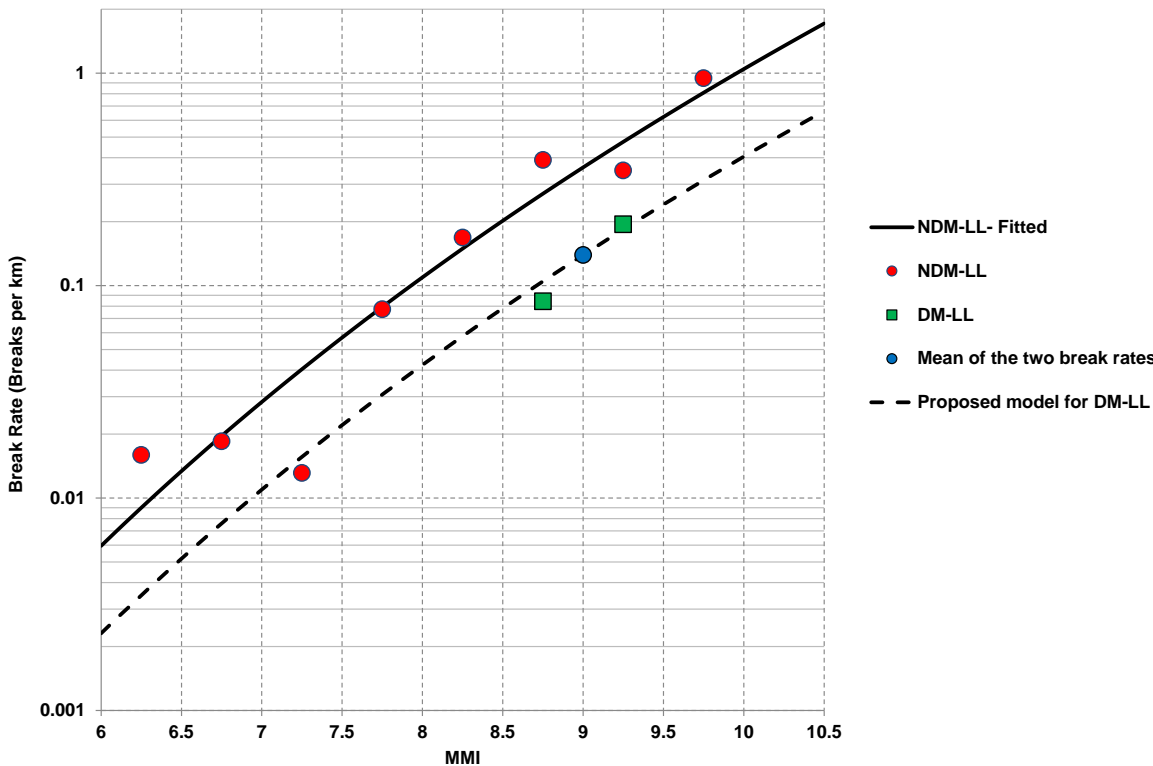


Figure 5.14 Proposed fragility curve for ductile mains in areas with little or no observed liquefaction.

Table 5.2 Parameters of the proposed new fragility curves derived using the D&R model to estimate shaking intensities for the Christchurch earthquakes (BR [km^{-1}] = $a \times \text{MMI}^b$).^b

Pipe Class	Ground Liquefaction Susceptibility	Class Code	a	b	R ²	Median	μ	σ
Ductile mains	Low	DM-LL	3.10e-11	10.116	-	-	-	-
	Moderate	DM-ML	-	-	-	0.55	0.55	0.18
	High	DM-HL	-	-	-	0.61	0.61	-
	Lateral Spreading	DM-LS	-	-	-	2.58	2.59	0.06
Non-ductile mains	Low	NDM-LL	8e-11	10.116	0.9032	-	-	-
	Moderate	NDM-ML	-	-	-	1.40	1.52	0.70
	High	NDM-HL	-	-	-	2.79	3.00	2.31
	Lateral Spreading	NDM-LS	-	-	-	5.42	6.21	5.33
Ductile sub-mains	Low	DSM-LL	3e-9	8.3389	0.9914	-	-	-
	Moderate	DSM-ML	-	-	-	0.46	0.42	0.23
	High	DSM-HL	-	-	-	0.61	0.61	0.53
	Lateral Spreading	DSM-LS	-	-	-	1.91	1.90	0.36
Non-ductile sub-mains (excluding galvanised iron)	Low	NDSM-LL	7.75e-9	8.3389	-	-	-	-
	Moderate	NDSM-ML	-	-	-	1.19	1.18	-
	High	NDSM-HL	-	-	-	2.79	3.02	-
	Lateral Spreading	NDSM-LS	-	-	-	4.02	4.55	-

Pipe Class	Ground Liquefaction Susceptibility	Class Code	a	b	R ²	Median	μ	σ
Galvanised iron submains	Low	NDSM-LL	2e-9	9.4409	0.8929	-	-	-
	Moderate	NDSM-ML	-	-	-	6.36	6.11	1.56
	High	NDSM -HL	-	-	-	8.51	8.50	0.37
	Lateral Spreading	NDSM -LS	-	-	-	10.85	10.86	3.30

5.2.2 Discussion

The accuracy of fragility models derived in this section were also affected by the following:

- The sporadic nature of liquefaction and the impact of that on the liquefaction susceptibility classification used.
- Uncertainties in the estimated ground motion intensities from the D&R MM-intensity attenuation model used to correlate pipe damage to ground shaking intensity.
- The multiple earthquakes in the CES made relating observed damage to a particular earthquake difficult.
- Insufficient data for discrete analysis of pipe types and sizes resulting in combining pipe size and type data into the four classes based on ductility and size (i.e. mains and sub-mains).

The fragility models developed using this methodology are simple and easy to use. The required input data to the models, liquefaction susceptibility and ground shaking intensity are relatively easy to make available. The required liquefaction susceptibility information is currently being compiled by GNS Science for all New Zealand, albeit at a coarse scale (1:250,000). The shaking MM intensities can be obtained by using the D&R MM attenuation model. The incorporation of these fragility curves into risk modelling procedures is a relatively quick and simple process that delivers a good estimation of the likely damage to pipes from an earthquake, whether immediately post-earthquake to help with recovery planning or pre-earthquake to help with making decisions to improve the resilience of pipe networks.

5.3 Comparison of Proposed New Fragility Models with Existing Fragility Models

5.3.1 The Cousins Model

The base case for estimating repair rates is large-diameter, modern, welded steel pipeline buried in ground that has negligible potential for liquefaction or landslide failure. On this basis, the equation for estimating the pipe repair rate is:

$$RR = K1 * K2 * K3 * K4 * K5 * RR_{GS} \quad \text{Equation 5.2}$$

where RR_{GS} (Equation 5.3) is the base repair rate (for ground shaking alone), and $K1$ to $K5$ are factors that allow for pipe material, coupling type and age, pipe size, landslide hazard and liquefaction hazard.

$$RR_{GS} = A \times 10^{B/(MMI-C)} \quad \text{Equation 5.3}$$

where, $A = 1600$, $B = -40$ and $C = 0.6$. The K factors are assumed to be 1.0, unless specified otherwise in Table 5.3. For example, (a) the factors for a welded steel pipeline, installed in 2000, of 1050 mm diameter and in good ground would be $1 \times 1 \times 1 \times 1 \times 1 = 1$, whereas (b) the combined factors for a steel pipeline with couplings, installed in 1953, of 250 mm diameter and on ground of high landslide hazard, with negligible liquefaction hazard, would be $1 \times 2 \times 4 \times 9 \times 1 = 72$.

Table 5.3 Relative fragility factors in the Cousins model.

Factor	Name	Conditions	Value
K1	Pipe Material Factor	Cast-Iron	2
K2	Coupling Age Factor	Couplings more than 50 years old	2
K3	Size Factor	Diameter < 400 mm	4
K4	Landslide Hazard Factor	Moderate	3
		High	9
		Extreme	27
K5	Liquefaction Hazard Factor	Moderate	3
		High	9
		Extreme	27

5.3.2 Comparison with the Cousins Model

To compare the mean break rate curves derived using the Cousins model with the mean break rate curves derived from Christchurch empirical data described in this report, the following assumptions were made when choosing damage enhancement factors from Table 5.3:

- Cousins' base model (large welded steel pipe in good ground) is larger than the pipes considered in this study; therefore, the size factor of 4 is applied to the Cousins base model.
- Most of the Christchurch mains are not older than 50 years and do not have coupling joints; therefore, the coupling age factor is not applied.

Incorporating the above assumptions into the Cousins model allowed comparing with the proposed new fragility models. The results are shown in Figure 5.15 and Figure 5.16.

The plots show that:

- Overall, break rates from the Cousins model are somewhat lower than the mean break rates from the model proposed here for the little or no liquefaction susceptibility category, particularly in the lower MM range. The lack of data in the Christchurch dataset for MM intensities less than MM8 may be influencing the lower end of the curve.

- In the moderate or greater (including lateral spreading) liquefaction susceptibility categories, pipe break rates show a two-fold response. Prior to the onset of liquefaction (i.e. below MM7) the Cousins curves are likely be more representative of the number of pipe breaks per kilometre. Once liquefaction has occurred (i.e. MM8 or greater) the number of pipe breaks per kilometre is constant, based on the Christchurch data. In areas of moderate or greater liquefaction susceptibility, the change could be modelled by modelling the onset of liquefaction at MM7 and taking a line from MM7 on the Cousins curve to intersect the constant Christchurch break-rates at MM8. This relationship, showing a transition from a break rate curve below MM7 to a constant break rate above MM8 in areas of moderate or greater liquefaction susceptibility, probably holds for all pipe sizes and types and so the same relationship potentially applies to the sub-mains category.

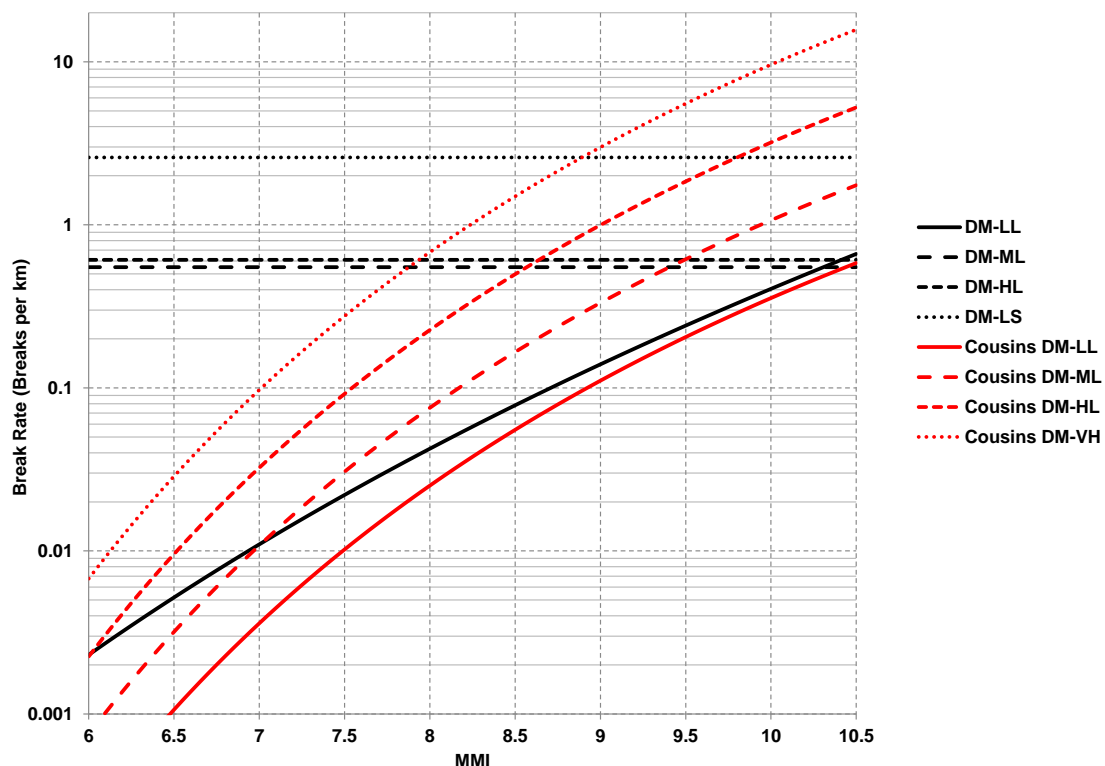


Figure 5.15 Comparison of the proposed models for ductile mains with the equivalent Cousins models.

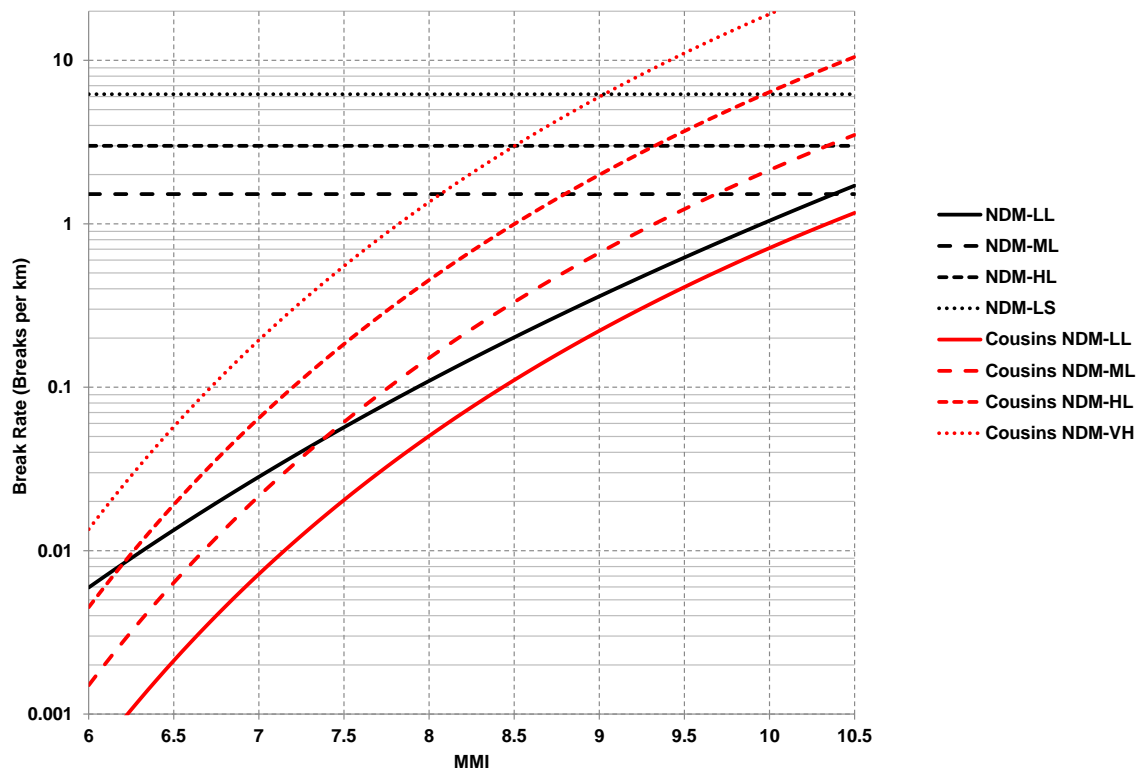


Figure 5.16 Comparison of the proposed models for non-ductile mains with the equivalent Cousins models.

6.0 LSN-BASED FRAGILITY FUNCTIONS

6.1 Introduction

To reduce some of the uncertainties and ambiguities around using Modified Mercalli intensity, it was necessary to derive fragility functions that are based on measurable parameters such as Peak Ground Acceleration (PGA) or Peak Ground Velocity (PGV), as well as use a well-accepted methodology for liquefaction susceptibility evaluation. In the following sections, an attempt has been made to enable this by correlating the observed damage to Liquefaction Severity Number (LSN).

6.2 PGAs of the Canterbury Earthquake Sequence

Peak ground acceleration (PGA) refers to the maximum ground acceleration measured across a specific directional plane during shaking. In this analysis, the horizontal PGA in both the principal directions were used. Ground motions were recorded by thirty GeoNet strong motion recording stations in the Canterbury region during the February and June earthquakes. The acceleration readings were used to find PGA recorded at each station, i.e. the highest acceleration measured from the two horizontal directions (usually north-south and east-west). These point PGAs were then used to create a smooth contoured map (Figure 6.1 and Figure 6.2) using ShakeMapNZ. ShakeMapNZ interpolates the PGA values in between stations using a least squared analysis; calculates the PGA, based on the distances from nearby stations; and adds a bias correction equation for larger distances (Horspool 2015).

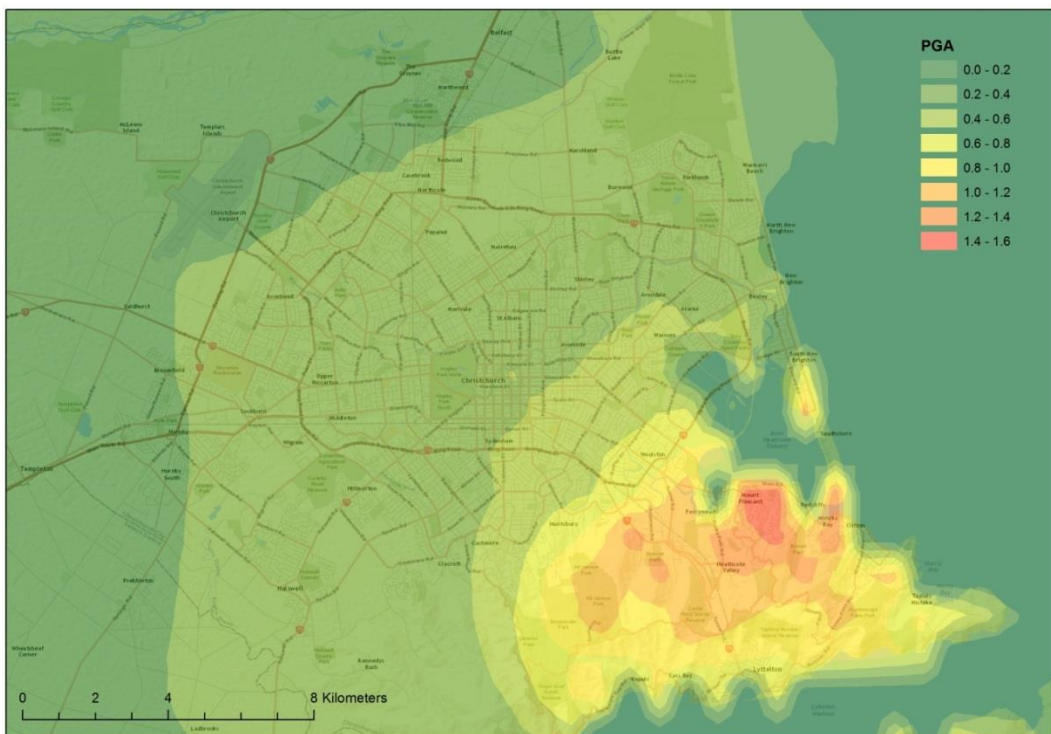


Figure 6.1 ShakeMapNZ produced PGA map of the February 22nd 2011 earthquake.

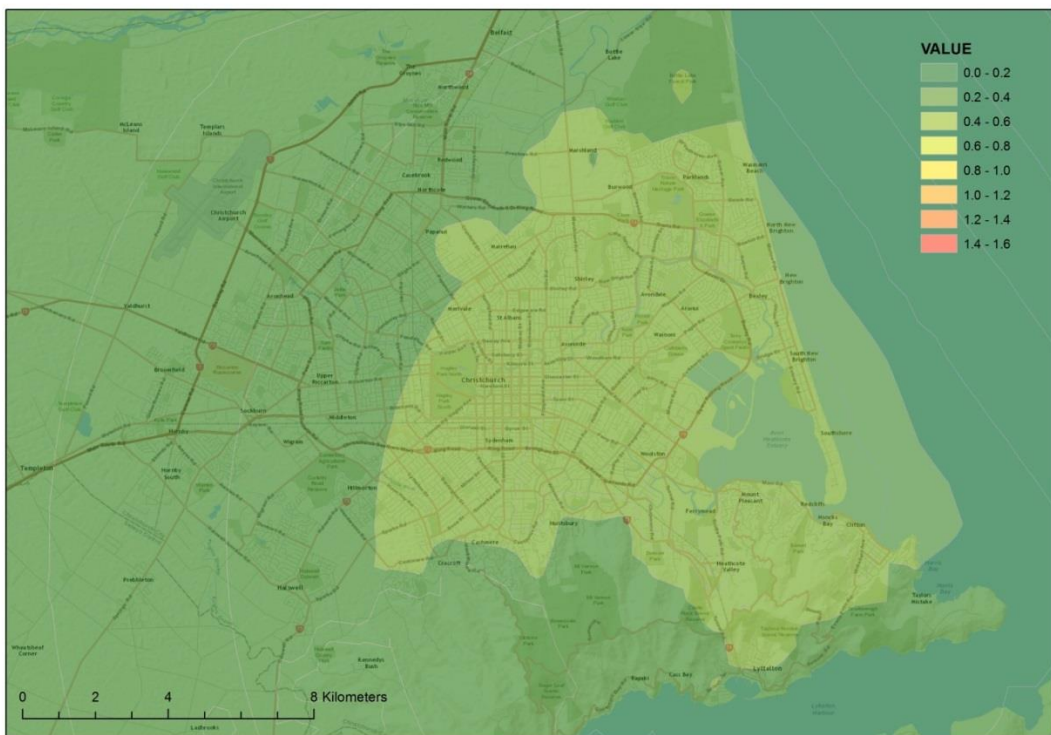


Figure 6.2 ShakeMapNZ produced PGA map of the June 13th 2011 earthquake.

It is evident from the maps that the February PGAs are much higher than the June PGAs (five times higher when comparing the maximums). This large difference in PGAs has contributed to much lower break rates observed in June (~four times lower as shown in Table 4.1).

6.3 Liquefaction Severity Number

Liquefaction Severity Number (LSN) is an index developed by Tonkin & Taylor Ltd that uses the geotechnical properties and groundwater conditions at a site to estimate the potential for liquefaction ground damage to occur for a given earthquake shaking intensity. It was developed using groundwater monitoring data and the Cone Penetration Test (CPT) data collected after the Canterbury earthquake sequence (2010–2016), calculated based on the earthquake shaking intensity and correlated with the observed ground damage.

LSN reflects calculated volumetric densification strain within different layers of soil, weighted by the depths of layers, as a proxy for likely severity of liquefaction land damage at the surface. The depth-weighting gives more weight to shallow liquefied layers to contribute to the surface damage than deeper layers. Since strains self-limit based on the initial relative density as the factor of safety drops, a given soil profile has a maximum LSN that it tends towards as the PGA that the layer is subjected to increases (Tonkin & Taylor 2013).

Measuring soil volumetric densification strain requires soil material properties. CPTs are usually carried out to measure soil resistance or shear strength. CPT involves forcing a cone and pipe sleeve, with known dimensions, vertically down through the soil, recording the properties of each soil layer in the soil profile that the cone goes through. The soil pore water pressure is also measured. Of particular interest to the CPT are shallow, low resistant soils with high pore water pressures. These soils are often highly susceptible to liquefaction and lead to increased damage to above- and underground assets during earthquakes. LSN is also dependant on the shaking level (PGA) and period of shaking, i.e. cyclic stress and number of

cycles, respectively. More details about LSN can be found in Tonkin & Taylor (2013) and van Ballegooij et al. (2014).

LSN maps for the February and June 2011 earthquakes were provided by Tonkin & Taylor Ltd as GIS raster files. Unfortunately, due to the distribution of the CPT locations, the LSN maps covered only about less than half of the city (Figures 6.3–6.5). This is because the maps rely on closely spaced CPTs to produce a good representation of liquefaction susceptibility. These CPTs were mostly located in the Residential Red Zone and areas with high degrees of observed liquefaction and land damage, with the aim of highlighting areas where there were known liquefaction issues; hence, enhanced foundation requirements had to be put in place for future developments. Therefore, not many CPTs were conducted in the western areas of Christchurch.

Overall, the LSN maps correlate well with the damage and liquefaction observed in Christchurch (highest LSNs are along the Avon River and in the Horseshoe Lake area in the eastern parts of the city). The February LSNs are higher compared to the June LSNs; this is due to multiple factors, including the difference in the PGAs and magnitudes of the events and the water table levels (the February earthquake occurred during summer and the June event during winter, when the water table was higher).

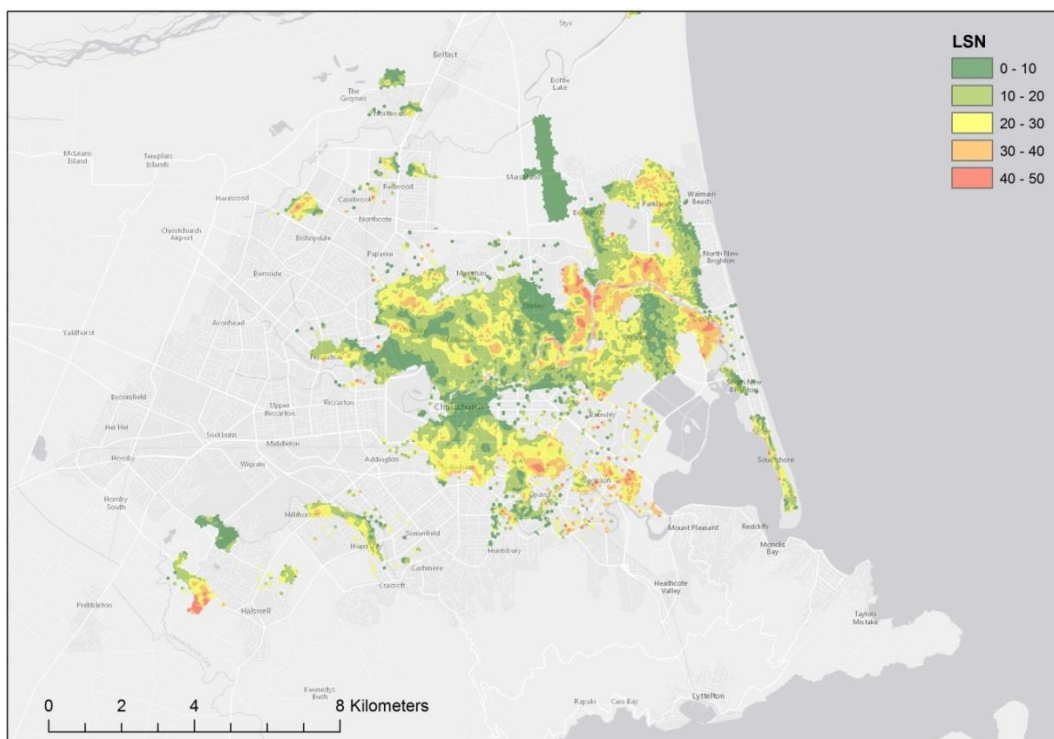


Figure 6.3 Smoothed LSN map (from Tonkin & Taylor Ltd) of Christchurch City for the February Mw 6.2 earthquake.

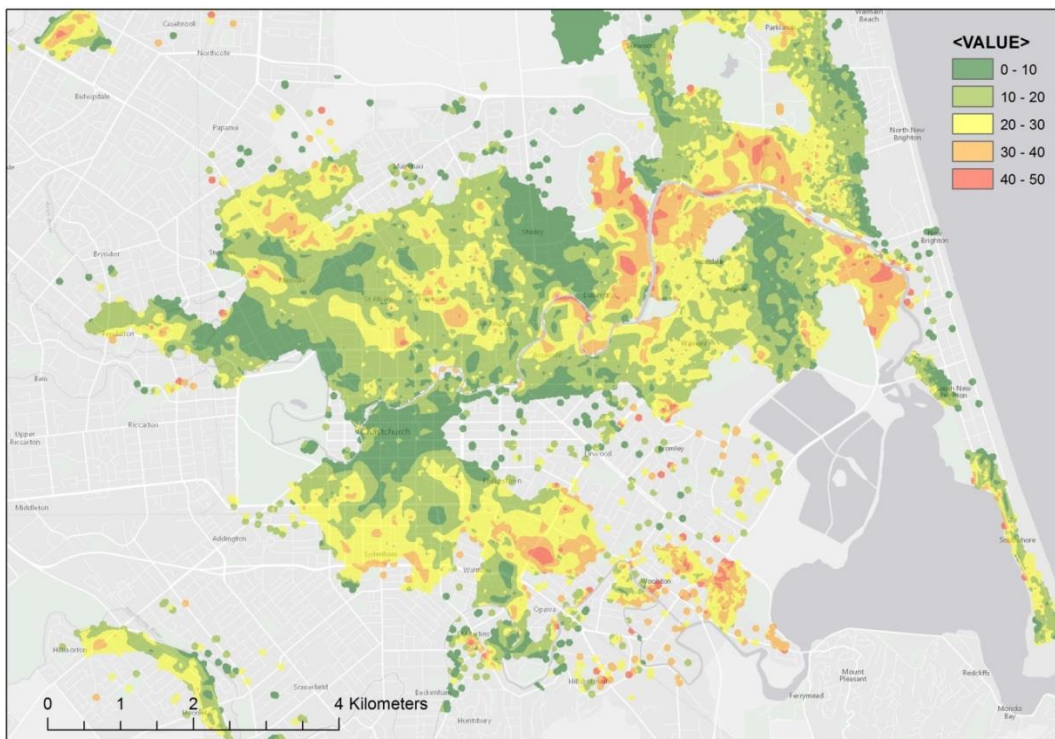


Figure 6.4 Smoothed LSN map (from Tonkin & Taylor Ltd) of the February Mw 6.2 earthquake, showing only the eastern suburbs in Christchurch.

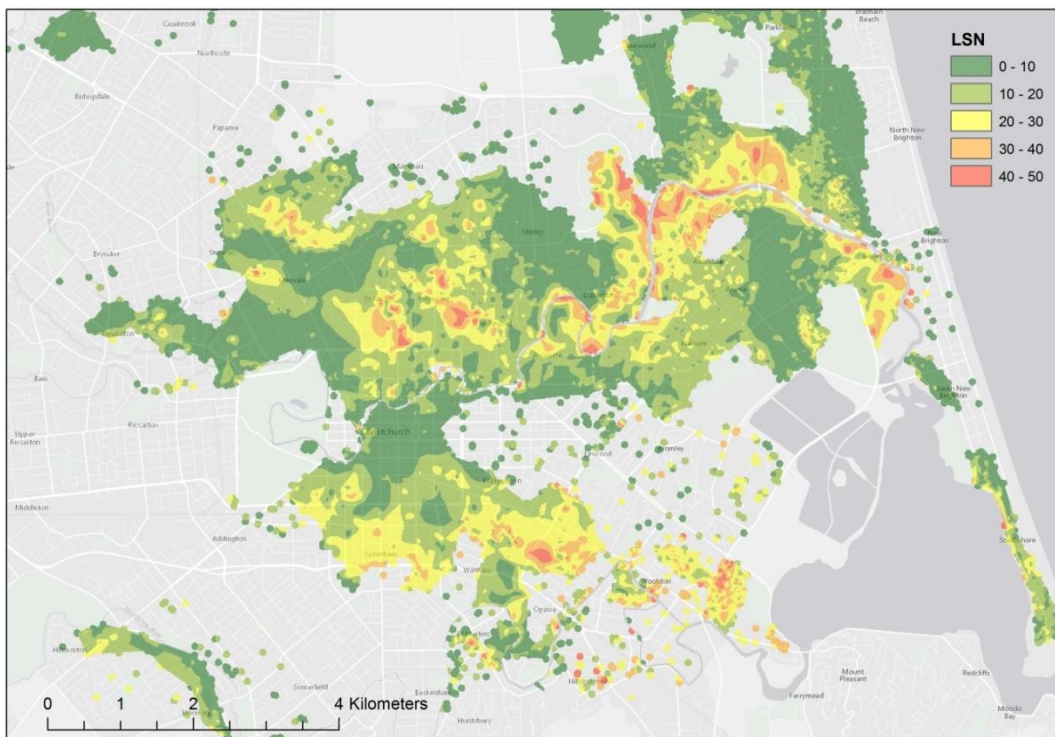


Figure 6.5 Smoothed LSN map (from Tonkin & Taylor) of Christchurch for the June Mw 6.3 earthquake.

6.4 Methodology

The approach followed to derive LSN-based fragility functions is similar to the one used to derive the MMI-based fragility models. The data preparation included the following steps:

- LSN maps for the September 2010, February 2011 and June 2011 earthquakes were obtained from Tonkin & Taylor Ltd as GIS raster files.
- The pipes were split into 20-metre or shorter segments (as some pipes are quite long and pass through different LSN or PGA zones).
- The segmented pipes were converted into points for further analysis. This was done by assuming segment centroids to represent pipe locations.
- The LSN information was spatially joined to the pipe centroid point data in ArcGIS.
- The PGA layers were also joined to the pipe network spatially so that each pipe centroid location was given the PGA value of the fixed PGA polygon that it fell inside.
- Finally, the pipe repair information provided by City Care Ltd was joined to the segmented pipes. The repair data, as mentioned before, was provided as points (i.e. at a location) where a pipe repair had been requested. The point repair data was joined to the pipe segments based on distance, i.e. the pipe closest to the repair location was assumed to be damaged.
- The combined dataset containing all the necessary LSN, PGA and repair data was then exported to an MS Excel spreadsheet for break rate calculations. There was not enough damage data from the September event to be included in the analysis, so the focus was put only on the repairs that were relevant to the February and June earthquakes.
- The calculated break rates were again screened using the criteria explained in Section 4.3.

6.5 Correlation of Pipe Damage with LSN

Figure 6.6 shows the pipe break rates for the range of LSNs calculated for the February and June events. The LSN values range from 0 to 45 and the break rates are calculated for each 5-unit interval and are placed in the middle of the interval. The figure reveals the following:

- As LSN increases, the break rates also generally increase. This is more evident in the February break rates, as there is a larger spread of LSN and a greater severity of damage. This can be expected as higher LSNs imply more severe liquefaction that will then cause more damage to the buried pipes.
- Break rates related to the February event are much higher than the June break rates. This is due to relatively more severe liquefaction and resulting damage to pipes during the February earthquake.
- The mains (diameter ≥ 100 mm) have sustained more damage compared to the sub-mains (diameter ≤ 100 mm), especially considering the damage from the February earthquake. Typically, larger pipes tend to be more robust and sustain less damage in an earthquake compared to smaller pipes like the sub-mains; however, in this case, the effect of pipe size on the break rates seems to have been cancelled by the effect of material type. That is, the mains in the pipe network were commonly made of non-ductile materials (susceptible to more damage) such as AC and CI, whereas the sub-mains were mainly made of ductile materials such as PE and PVC.

- In the very low and very high end of the LSN range, shown in Figure 6.6, there appears to be some inconsistency with the increasing trend in the break rates with increasing LSN. This implies that when there is no liquefaction (in the very low LSN range) or when there is lateral spreading (in the very high LSN range), LSN may not be a good metric to measure the extent of damage (as it is meant to gauge the extent of liquefaction only).
- The extent or coverage of the LSN maps also play a part here, as less than half of the city was mapped for LSN. This means that the break rates may not well-represent how the entire network performed, especially given the LSN maps cover the most affected areas. This may skew the break rates.

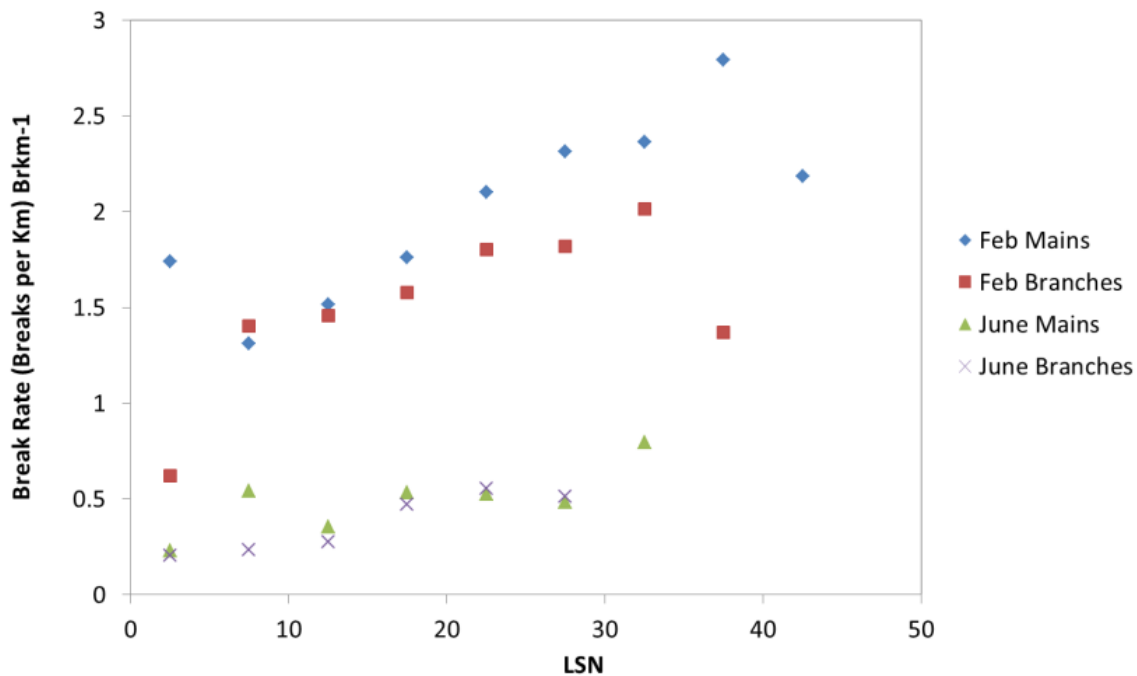


Figure 6.6 Relationship between Christchurch water supply break rates and LSN.

6.5.1 Screening Criteria

As explained in Section 4.4, removing biased and incorrect break rates from the damage dataset by applying a screening criterion is important. Very high break rates may arise from very small sample sizes. For example, a pipe class with a total length of only 100 m, and with one failure, is recorded to have 10 breaks per km (due to scaling).

A comparison of the unscreened data with the screened data showed that most of the very high break rates are filtered out when the screening criteria is applied. Also, no obvious pattern or relationship could be established between break rate, PGA, LSN or material type when unscreened break rates are considered. The screening criteria used for the above comparison was to have 95% confidence that the break rates are within 50% of the ‘true’ repair rate. However, the confidence level was later lowered to 90% to allow more break rate data points to pass the screening criteria.

6.5.2 Combing Data into Broader LSN Bands

The break rates were re-calculated for the same four pipe classes considered in the previous section (i.e. ductile mains, non-ductile mains, ductile sub-mains and non-ductile sub-mains) and for three LSN ranges: 0–16, 16–25 and 25+ bins. The three LSN bins used for this purpose

were originally suggested by van Ballegooij et al. (2014) for none-to-minor, minor-to-moderate, and moderate-to-severe liquefaction-induced damage incurred from the CES. Having broad bins such as these, rather than many small bins, means larger sample sizes are formed in each pipe class and bin, thus increasing the chances of getting more data points to pass the screening criteria. However, the additional data come at the cost of averaging out some of the effect of LSN on break rate as, for example, an LSN of 1 is put in the same category as an LSN of 15.

It is also worth mentioning that LSN shows the probability of damage and severity of liquefaction. This means that it is possible for severe liquefaction to occur at low LSNs. However, that has a very low probability. Therefore, although the above LSN cut-off points do not fully represent the occurrence of liquefaction, they are good approximations of the overall liquefaction severity expected.

6.5.3 Separating Lateral Spreading Damage

LSN does not provide a very good indication of lateral spreading as it does not consider three-dimensional effects, dynamic response, proximity of free faces or soil ejecta loss to the surface (van Ballegooij et al. 2014).³ Moreover, when lateral spreading occurs, it multiplies the resulting break rates due to lateral movement shearing and pulling out pipe joints, etc. (O'Rourke et al. 2014). It has a much greater impact on buried pipes than liquefaction alone (Section 5.2.1), although the effect may not be as wide spread as in liquefaction. Therefore, it was necessary to separate the areas affected by lateral spreading from the rest of the study area. This was done by separating Classes 5 and 6 (moderate-to-major lateral spreading and severe lateral spreading) of the observed liquefaction maps (see Section 2.2) into 'Lateral Spreading' class.

6.5.4 Extrapolation of the LSN Maps

As discussed in Section 6.3, the LSN maps covered less than half of the city, focusing largely on the badly damaged areas. This could potentially skew the break rates estimated for the different LSN bins and result in overestimation of damage. Therefore, it was necessary to include the less affected parts of the water network in the analysis to represent the damage more accurately. This required the LSN maps to be extended. Extending the LSN maps also provided more data (i.e. increased sample sizes in each LSN bin).

The LSN maps were extended by assigning an LSN to each pipe segment outside the original LSN maps. The assignment of LSNs was guided by the observed liquefaction (Section 2.2) and the estimated PGA at the pipe centroid location for each event. A degree of judgement was also required.

It is also worth mentioning that the June observed liquefaction map covered a wider area compared to the February map. Thus, the June liquefaction map was used for the areas not covered by the February map, especially the western suburbs (Figure 6.7). However, as discussed previously, the February event was more damage-causing than the June event, even at similar shaking intensities due to the greater extent of liquefaction. Therefore, the following assumptions had to be made to enable the assignment of LSNs:

³ Research is ongoing to predict and classify the severity of lateral spreading using the post-liquefaction reconsolidation settlement index (S_{v1D}), distance to nearby water bodies and the water depth in them.

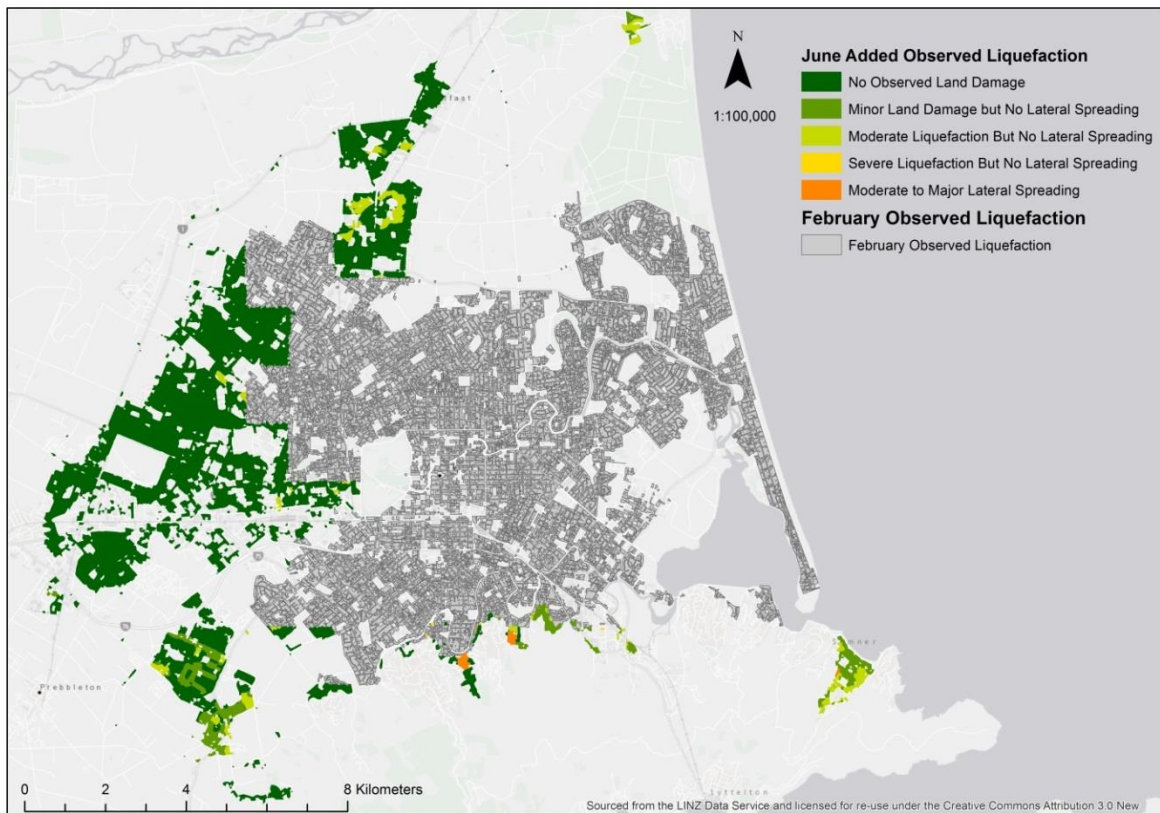


Figure 6.7 Areas surveyed for surface liquefaction manifestation following the June event but not inspected post-February earthquake (Canterbury Geotechnical Database 2013).

Assumption 1: Since the Christchurch City experienced PGAs of at least 0.1 g during both events, it is assumed that the areas not affected by liquefaction during the June earthquake would have also not experienced liquefaction in the February earthquake. This is because, at shaking intensities of over 0.1 g, susceptible soils always show some signs of liquefaction. Therefore, if there was no observed liquefaction in an area in June, it was assumed that the area did not liquefy in the February earthquake, even if the shaking intensity was higher.

Assumption 2: The pipes that were located outside the February LSN map extent, but were inside the February observed liquefaction map, were given LSN values that directly relate to the February observed liquefaction severity map. That is, the pipes in regions of none-to-low liquefaction (Classes 0, 1 and 2 of the observed liquefaction map) were placed in the low LSN category (0–16), the pipes in moderately liquefied areas (Class 3) were placed in the medium LSN range (16–25) and the pipes in the high liquefaction category (Class 4) were placed in the high LSN range of 25+. As explained above, pipes in the areas mapped as affected by lateral spreading (Classes 5 and 6) were placed in the lateral spreading category (Table 6.1). The same rules applied to the June observed liquefaction map when assigning a likely LSN range to pipes that fell outside the June LSN map extent.

Table 6.1 Relationship of Tonkin & Taylor Ltd observed liquefaction categories with LSN classes for the unaltered part of the February and June LSN maps.

Observed Liquefaction Map Class	Observed Liquefaction Map Category	LSN Range Assumed
Class 0	Not observed; presumed no land damage	0–16
Class 1	No land damage	0–16
Class 2	Minor land damage but no liquefaction	0–16
Class 3	Moderate liquefaction but no lateral spreading	16–25
Class 4	Severe liquefaction but no lateral spreading	25+
Class 5	Moderate to major lateral spreading	Lateral spreading
Class 6	Severe lateral spreading	Lateral spreading

Assumption 3: LSN numbers follow a distinguishable pattern in relation to PGA. For PGAs of 0–0.1 g there is usually no evidence of liquefaction (very low LSNs), for 0.1–0.3 g a steep gradient and increase in liquefaction severity is observed, and for values above 0.3 g there is a plateau in LSN (Figure 6.8). Since the June PGAs were generally in the range of 0.1–0.3 g, most parts of the city did not experience its maximum liquefaction damage in this event. Therefore, if the soil were to experience higher PGAs as in the February event, the severity of liquefaction could have potentially been higher. Thus, in order to replicate the increase in LSN (or liquefaction damage) as a result of higher PGAs (0.0–0.2 g in June compared to 0.2–0.4 g in February), pipes in Class 2 (minor land damage but no liquefaction observed in the June event) were placed in the LSN category 16–25 instead of 0–16, and Class 3 (moderate liquefaction but no lateral spreading observed in the June event) were moved up to the 25+ LSN category to extend the February LSN map (Table 6.2).

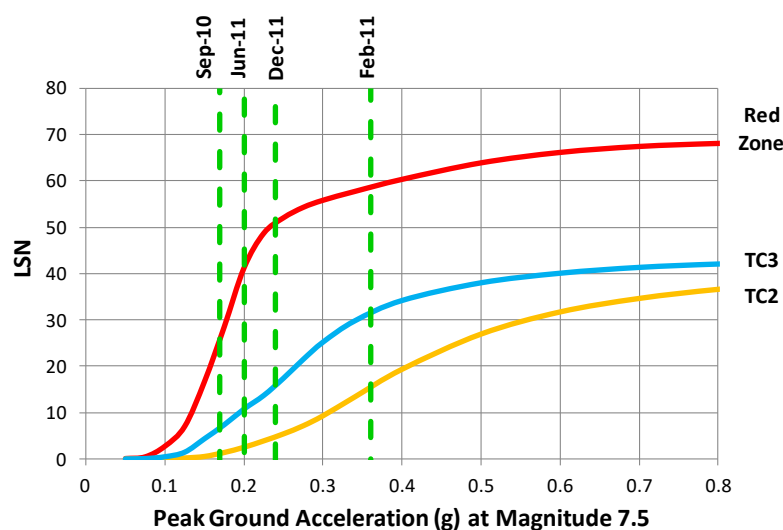


Figure 6.8 Sensitivity of LSN to magnitude-weighted PGA for Christchurch residential Red Zone (major damage), TC3 (moderate liquefaction damage) and TC2 (minor damage) (van Ballegooij et al. 2014).

Table 6.2 Relationship of Tonkin & Taylor Ltd observed liquefaction categories for the June event with LSN classes assumed for the extended part of the February LSN map.

Observed Liquefaction Map Class	Observed Liquefaction Map Category	LSN Range Assumed
Class 0	Not observed; presumed no land damage	0–16
Class 1	No land damage	0–16
Class 2	Minor land damage but no liquefaction	16–25
Class 3	Moderate liquefaction but no lateral spreading	25+
Class 4	Severe liquefaction but no lateral spreading	25+
Class 5	Moderate to major lateral spreading	Lateral spreading
Class 6	Severe lateral spreading	Lateral spreading

Assumption 4: Observed liquefaction Classes 5 and 6 remained the same (Table 6.1 and Table 6.2). This is because it is assumed that all areas affected by lateral spreading were mapped in both June and February observed liquefaction maps.

The extended LSN maps for both the events are shown in Figure 6.9 and Figure 6.10. A significant portion of the additional data from the areas that were not mapped originally fell in the lower LSN categories. This was expected because most of the unmapped western areas of Christchurch had lower liquefaction severity compared to the other parts of the city. The additional data also helped by adding data in areas that experienced PGAs above 1 g, giving a better understanding of the effect of pure shaking on the pipes in such areas.

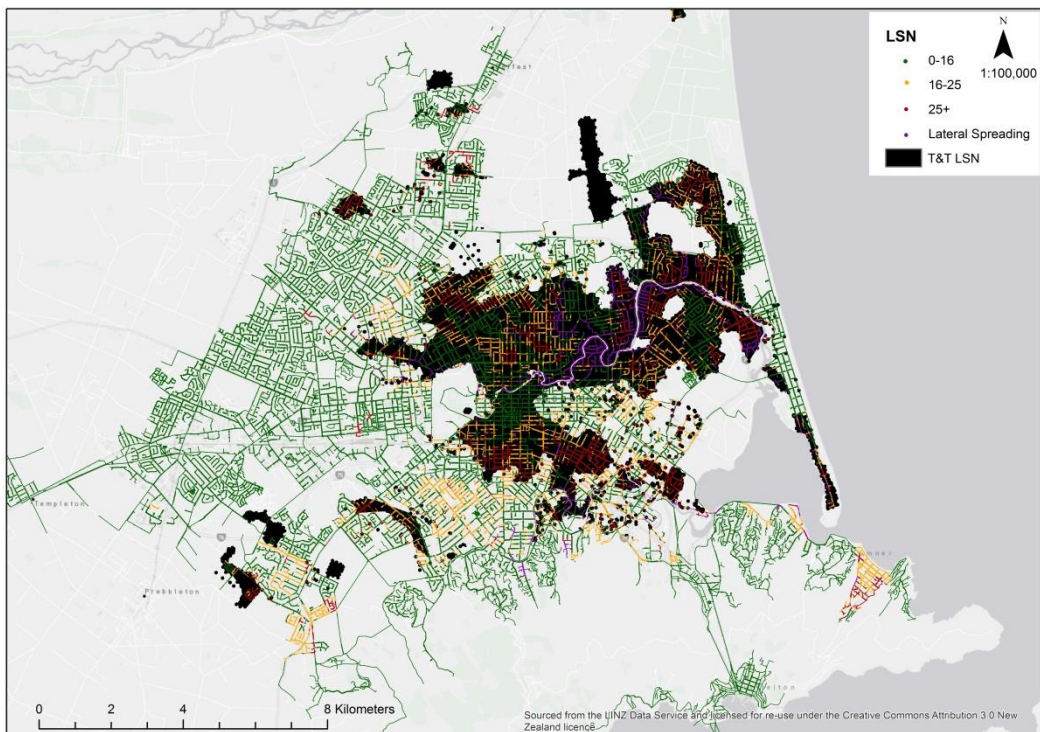


Figure 6.9 Christchurch water supply pipes in the 'Low', 'Medium' and 'High' LSN ranges in the February event. The black shaded area represents the extent of the original LSN map from Tonkin & Taylor Ltd.

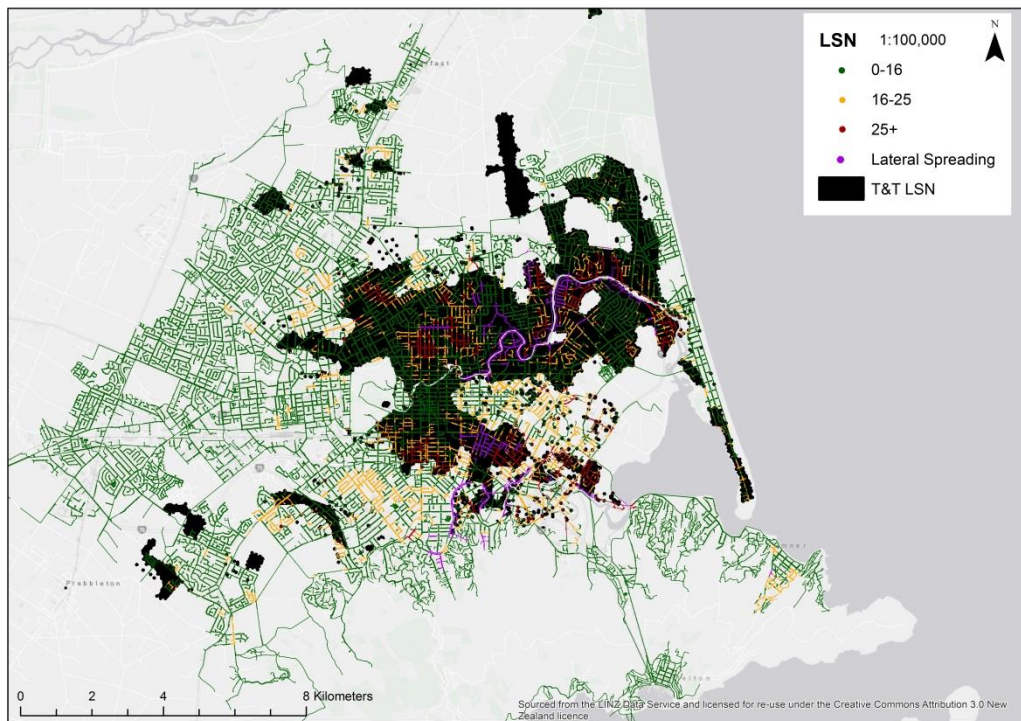


Figure 6.10 Christchurch water supply pipes in the 'Low', 'Medium' and 'High' LSN ranges in the June event. The black shaded area represents the extent of the original LSN map from Tonkin & Taylor Ltd.

6.5.5 Final Break Rates

Break rates for the four pipe classes (i.e. ductile and non-ductile mains, ductile sub-mains and galvanised iron sub-mains) were calculated by dividing the total number of breaks by the total length in each of the three LSN categories (i.e. 0–16 or ‘Low’, 16–25 or ‘Medium’, and 25+ or ‘High’), as well as for the lateral spreading class. The break rates in each case were calculated using:

- a. LSN data from the original Tonkin & Taylor Ltd maps only, and
- b. LSN data from both the original maps and the extensions added.

For the first case above, as detailed LSN maps were available, it was possible to calculate the break rates for LSNs from 0 to 45 with 10-unit intervals. The resulting break rates are shown in Figures 6.11–6.14, and tabulated in Tables 6.3–6.6.

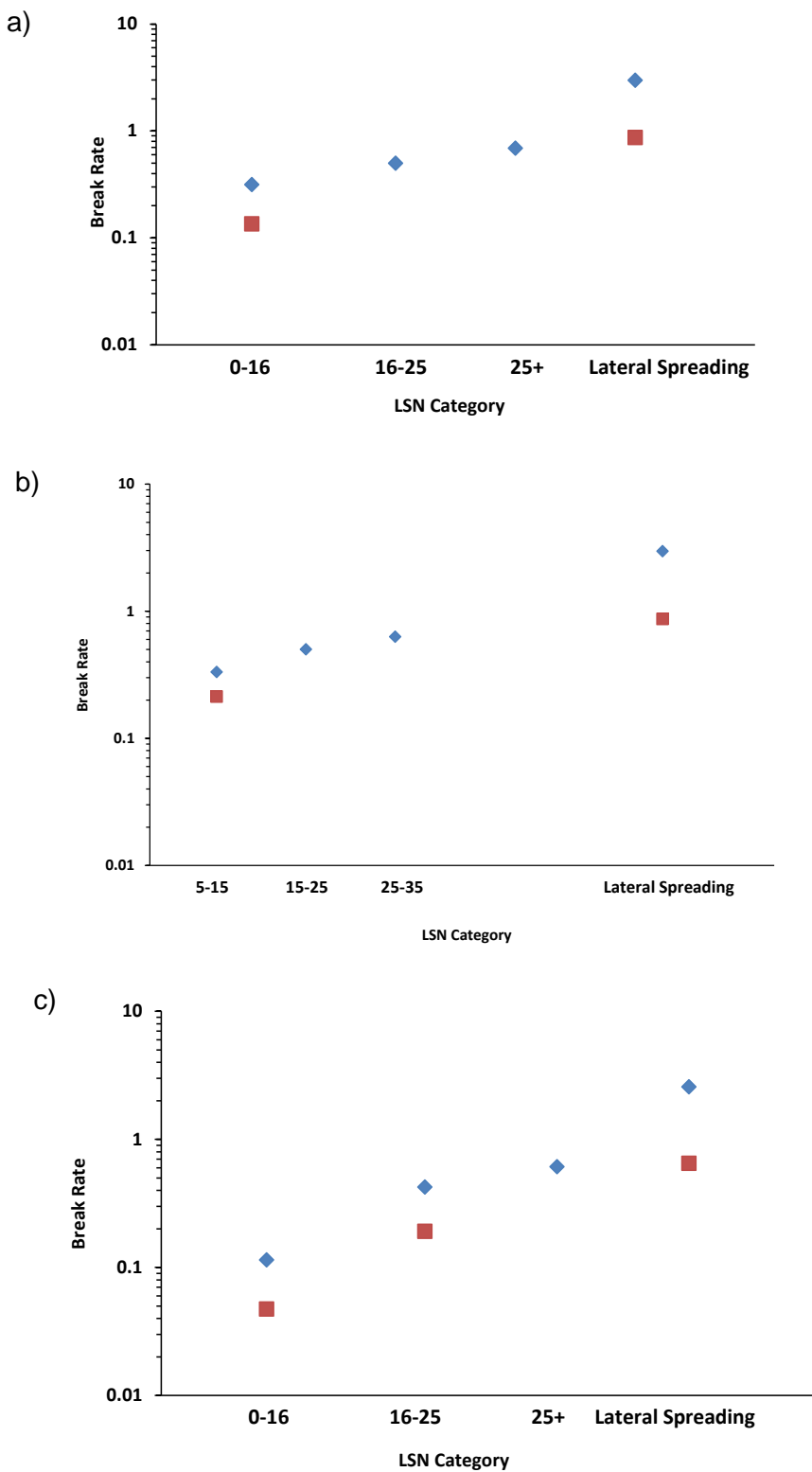


Figure 6.11 Break rates for ductile mains, comparing the damage due to the February 2011 earthquake (blue points) with the June 2011 earthquake damage (red points). a) and b) contain information from the original Tonkin & Taylor Ltd LSN maps only, and c) includes information from the extended LSN maps.

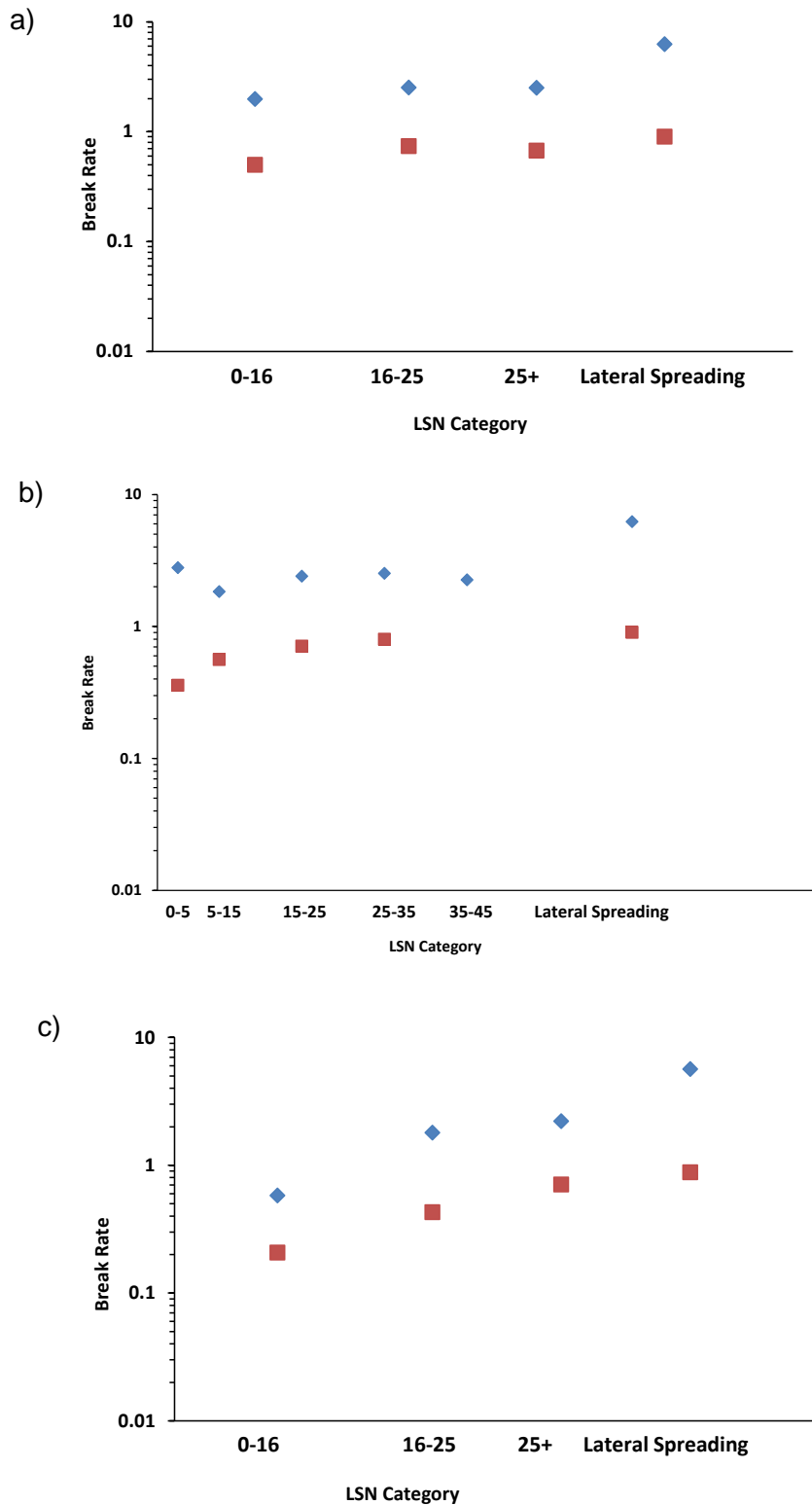


Figure 6.12 Break rates for non-ductile mains, comparing the damage due to the February 2011 earthquake (blue points) with the June 2011 earthquake damage (red points). a) and b) contain information from the original Tonkin & Taylor Ltd LSN maps only, and c) includes information from the extended LSN maps.

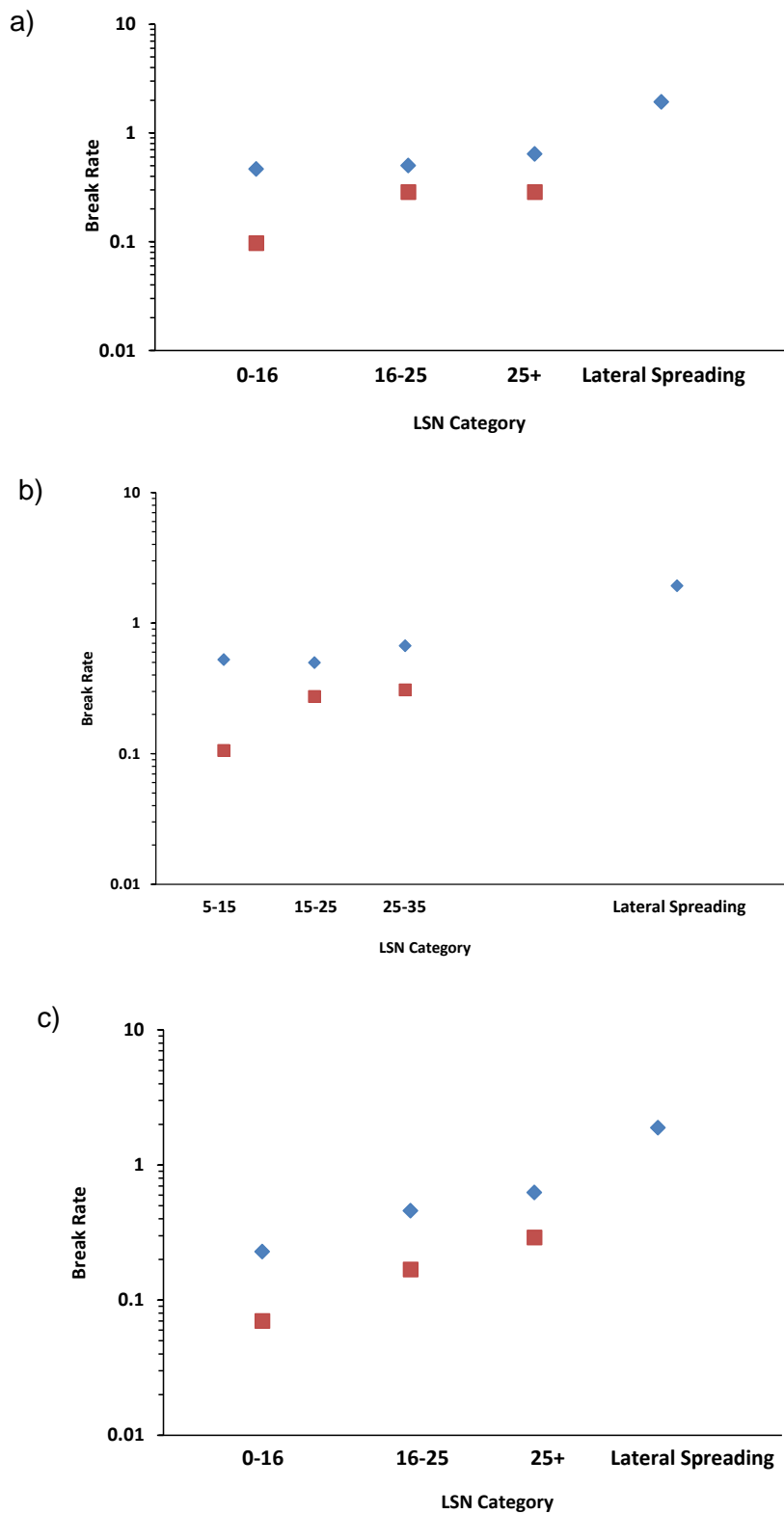


Figure 6.13 Break rates for ductile sub-mains, comparing the damage due to the February 2011 earthquake (blue points) with the June 2011 earthquake damage (red points). a) and b) contain information from the original Tonkin & Taylor Ltd LSN maps only, and c) includes information from the extended LSN maps.

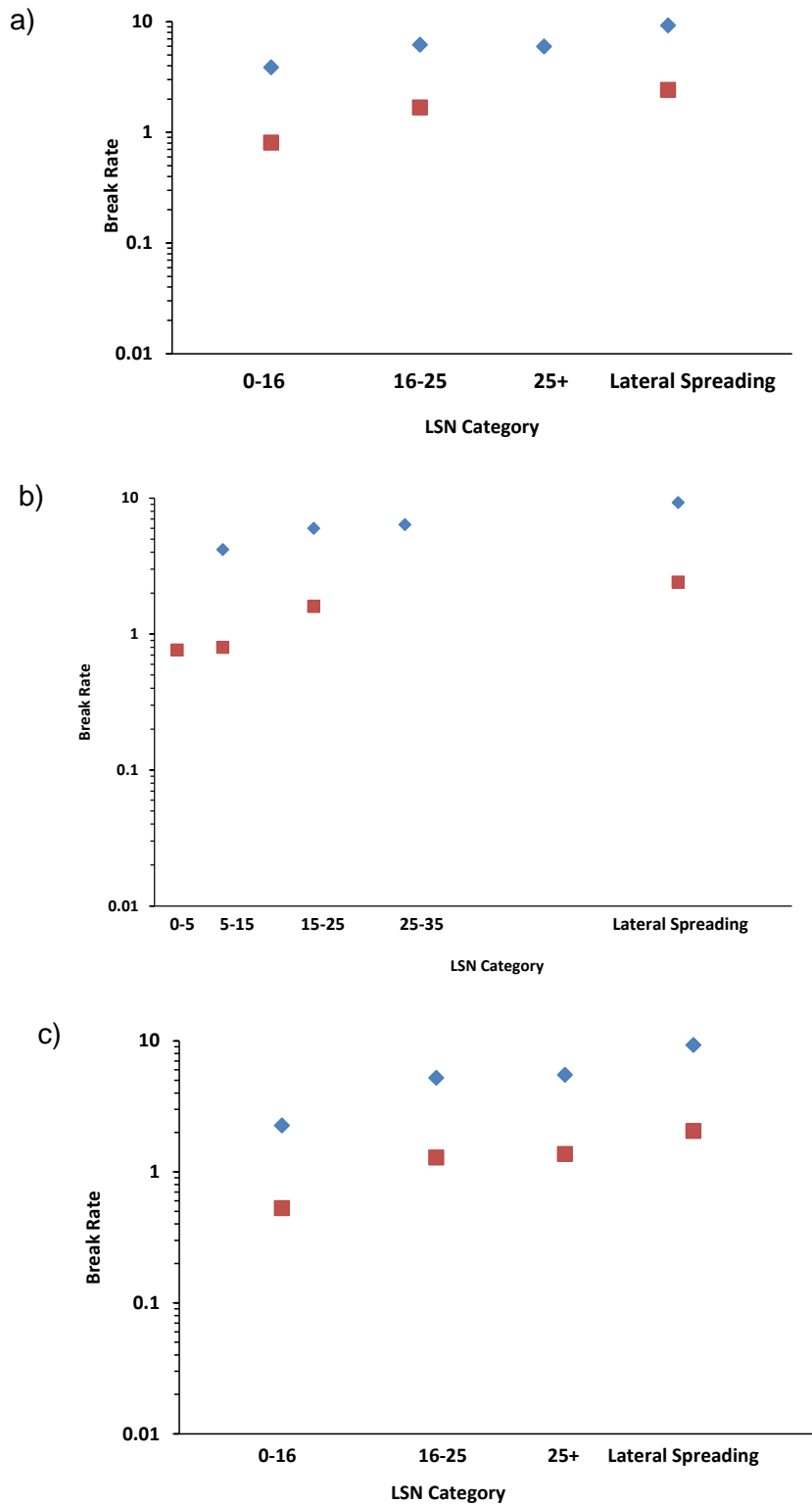


Figure 6.14 Break rates for galvanised iron sub-mains, comparing the damage due to the February 2011 earthquake (blue points) with the June 2011 earthquake damage (red points). a) and b) contain information from the original Tonkin & Taylor LSN maps only, and c) includes information from the extended LSN maps.

Table 6.3 Break rates for ductile and non-ductile mains, ductile sub-mains and galvanised sub-mains in Christchurch for the February and June events, calculated for broader LSN ranges using LSNs from the original Tonkin & Taylor Ltd LSN maps only.

LSN	Ductile Mains		Non-Ductile Mains		Ductile Sub-Mains		Galvanised Iron Sub-Mains	
	June	Feb	June	Feb	June	Feb	June	Feb
0–16	0.14	0.31	0.50	1.97	0–16	0.14	0.31	0.50
16–25	-	0.50	0.74	2.50	16–25	-	0.50	0.74
25+	-	0.69	0.67	2.49	25+	-	0.69	0.67
LS	0.87	2.96	0.90	6.22	LS	0.87	2.96	0.90

Table 6.4 Break rates for ductile and non-ductile mains, ductile sub-mains and galvanised iron sub-mains in Christchurch for the February and June events, calculated for finer LSN ranges using LSNs from the original Tonkin & Taylor Ltd LSN maps only.

LSN	Ductile Mains		Non-Ductile Mains		Ductile Sub-Mains		Galvanised Iron Sub-Mains	
	June	Feb	June	Feb	June	Feb	June	Feb
0–5	-	-	0.36	2.79	-	-	0.76	-
5–15	0.21	0.33	0.56	1.84	0.11	0.53	0.80	4.18
15–25	-	0.50	0.71	2.40	0.27	0.50	1.60	5.98
25–35	-	0.63	0.80	2.53	0.31	0.67	-	6.38
35–45	-	-	-	2.25	-	-	-	-
LS	0.87	2.96	0.90	6.22	-	1.93	2.41	9.27

Table 6.5 Break rates for ductile and non-ductile mains, ductile sub-mains and galvanised iron sub-mains in Christchurch for the February and June events, calculated for broader LSN ranges using LSNs from the extended LSN maps.

LSN	Ductile Mains		Non-Ductile Mains		Ductile Sub-Mains		Galvanised Iron Sub-Mains	
	June	Feb	June	Feb	June	Feb	June	Feb
0–16	0.05	0.11	0.21	0.58	0.07	0.23	0.53	2.26
16–25	0.19	0.42	0.43	1.80	0.17	0.46	1.29	5.21
25+	-	0.61	0.70	2.21	0.29	0.62	1.36	5.49
LS	0.65	2.57	0.88	5.65	-	1.88	2.05	9.30

Table 6.6 Ratio of break rates calculated for broad LSN ranges based on the original LSN maps (Table 6.3) over the break rates calculated using the extended LSN maps (Table 6.5).

LSN	Ductile Mains		Non-Ductile Mains		Ductile Sub-Mains		Galvanised Iron Sub-Mains	
	June	Feb	June	Feb	June	Feb	June	Feb
0–16	-65	-63	-58	-71	-28	-51	-35	-42
16–25	-	-14	-42	-28	-41	-9	-23	-16
25+	-	-11	5	-11	2	-3	-	-8
LS	-25	-13	-2	-9	-	-2	-15	0

The following observations are made by comparing the break rates in the above tables:

- Break rate increases with increasing LSN. This is expected as LSN is a measure of soil settlement (or permanent ground displacement) that has been shown to correlate well with damage to buried pipes in the presence of liquefaction (O'Rourke et al. 2014).
- All pipes affected by lateral spreading have substantially higher break rates than those affected by liquefaction (2.2–4.1 times higher than the high LSN category, based on the averages of break rates for each pipe category in Table 6.5).
- The June break rates are 20–50% lower than the February break rates (see Table 6.5). This, as explained in Section 4.5, is consistent with the lower liquefaction severity and relatively limited damage observed in June earthquake. This could also be because most weak points in the network had already suffered damage during the February earthquake.
- When comparing the break rates across different pipe types, it is seen that the larger pipes (mains) have lower break rates than smaller pipes (sub-mains). This is because the larger pipes generally have superior joints, more sophisticated installation techniques and are frequently maintained.
- Non-ductile mains have break rates that are 2–5 times higher than the ductile mains. Same comparison cannot be done between ductile sub-mains and galvanised iron sub-mains because of the major differences in size and material types in the two groups.
- Break rates calculated for the three LSN ranges defined (based on the extended LSN maps) are in general lower than the ones calculated using the original LSN maps. This is mainly due to having larger sample sizes without the same level of damage observed in the added parts. This shifts the focus to calculate break rates from not just the worst affected parts of the network but from the whole network, including the parts that performed better. This will give a more realistic picture of how the network performed (see Table 6.6).
- Break rates calculated for the high LSN range based on the original LSN maps and the extended ones are broadly similar (only up to 10% difference with the ones based on the extended maps being lower), but the break rates for the medium and low LSN ranges based on the extended maps are 10–40 and 30–70% lower than the ones based on the original maps, respectively. This is expected, given that most of the parts added to the original LSN maps fell into the lowest LSN category, followed by the medium LSN category, resulting in larger sample sizes in both the categories with not as much damage and, hence, lower overall break rates. This effect is more evident in the low LSN category, as most of western Christchurch fell into this category, significantly increasing the sample size with not much damage in these areas. For the high LSN category, there are only some small additional areas mapped as having 25+ LSNs in the Sumner and Redwood areas of Christchurch.
- There is also about 2–25% reduction in the break rates for the lateral spreading category. This is due to addition of the areas that had lateral spreading in the February or June events but were outside the original LSN maps (i.e. Beckenham along the Heathcote River, and some coastal areas in Mount Pleasant and Redcliffs).

One observation that needs further clarification is on the increase in break rates in the lowest LSN range when smaller LSN intervals are used (Panel 'b' in Figure 6.12 and Figure 6.13). The high break rate is a result of other more important contributing factors than the influence of negligible liquefaction (which is expected at lower LSNs). In the absence of permanent ground motions because of liquefaction or lateral spreading, pipe damage is due to transient

motions. This suggests that, in the absence of liquefaction or lateral spreading potential, LSN does not correlate well with damage. It has been shown in the literature that, in such cases, Geometric Mean Peak Ground Velocity correlates well with damage to buried pipes (O'Rourke et al. 1999). For the other LSN categories (i.e. Medium and High) and the lateral spreading class, the break rates derived from damage data related to June and February events (see Panel 'c' of Figures 6.11–6.14, also summarised in Table 6.5) are suggested to be used for pipe damage modelling until more damage data becomes available from future earthquakes.

7.0 CONCLUSIONS

This report combined the invaluable pipe damage data that the Canterbury Earthquake Sequence provided with the globally existing damage data on pipes and proposed new pipe fragility models for modelling damage to buried water pipes in earthquakes, especially under the influence of liquefaction. The fragility models are based on damage data that were screened systematically to ensure the performance of pipes was well captured. As with most empirical fragility models, the proposed models are not well-supported by data and, in the case of the MMI-based fragility models, inherit the subjective-ness of the MMI scale. However, the models developed can be considered superior to existing models and can be used to better understand the likely performance of buried pipes when subjected to earthquake actions.

8.0 ACKNOWLEDGMENTS

Many individuals and organisations have contributed to the work presented in this report: SCIRT, Christchurch City Council, City Care Ltd, Opus Research, Jim Cousins, Andrew King, Tatiana Goded (all from GNS Science) and Sjoerd van Ballegooij (of Tonkin & Taylor Ltd). Their comments and suggestions on various matters related to the project are gratefully acknowledged. Dr ShengLin Lin and Sally Dellow from GNS Science are thanked for reviewing this report.

The funding provided by the New Zealand Ministry of Business, Innovation and Employment (MBIE) that enabled this research is gratefully acknowledged. The authors are also thankful to GNS Science for providing co-funding through the ‘Post-Earthquake Functioning of Cities’ and ‘RiskScape’ research programmes.

9.0 REFERENCES

- [ALA] American Lifelines Alliance. 2001. Seismic fragility formulations for water systems. Part 1, Guideline. Part 2, Appendices. [Washington (DC)]: American Lifelines Alliance. 2 vols.
- [ALA] American Lifelines Alliance. 2005. Seismic guidelines for water pipelines. [Washington (DC)]: American Lifelines Alliance. 1 vol. G & E Report 90.01.01, Rev. 0.
- Allen TI, Wald DJ, Worden CB. 2012. Intensity attenuation for active crustal regions. *Journal of Seismology*. 16(3):409–433. doi:10.1007/s10950-012-9278-7.
- Canterbury Geotechnical Database. 2013. Liquefaction and lateral spreading observations. *Map Layer CGD0300*. [Wellington (NZ): MBIE]; [accessed 2015 Jul 4].
<https://canterburygeotechnicaldatabase.projectorbit.com>
- Christchurch City Council. 2013. Wastewater facts and figures. Christchurch (NZ): Christchurch City Council; [accessed 2015 May 5]. <https://ccc.govt.nz/services/water-and-drainage/wastewater/about-wastewater/facts-and-figures>
- Cousins WJ. 2013. Wellington without water: impacts of large earthquakes. Lower Hutt (NZ): GNS Science. 124 p. (GNS Science report; 2012/30).
- Cox S. 2015. Did artesian water have an effect on the liquefaction damage in Christchurch? Lower Hutt (NZ): GNS Science. *New Zealand Natural Hazards Research Platform Presentation Series*. 23 February 2015.
- Cubrinovski M, Hughes M, Rourke T. 2014. Impacts of liquefaction on the potable water system of Christchurch in the 2010–2011 Canterbury (NZ) Earthquakes. *Journal of Water Supply: Research and Technology – AQUA*. 63(2):95–105. doi:10.2166/aqua.2013.004.
- Cubrinovski M, Hughes M, Bradley BA, McCahon I, McDonald Y, Simpson H, Cameron R, Christison M, Henderson B, Orense RP, et al. 2011. Liquefaction impacts on pipe networks: short term recovery project no. 6, Natural Hazards Research Platform. Christchurch (NZ): University of Canterbury; [accessed 2015 Jun 30].
<http://ir.canterbury.ac.nz/handle/10092/10178>
- Dowrick DJ, Rhoades DA. 2005. Revised models for attenuation of modified Mercalli intensity in New Zealand earthquakes. *Bulletin of the New Zealand Society for Earthquake Engineering*. 38(4):185–214.

- Eidinger J, Tang AK, editors. 2012. Christchurch New Zealand earthquake sequence of Mw 7.1 September 04, 2010 Mw 6.3 February 22, 2011 Mw 6.0 June 13, 2011: lifeline performance. Reston (VA): American Society of Civil Engineers. 327 p. (Technical Council on Lifeline Earthquake Engineering monograph; 40). February 2012 Revision 0.
- Goded T, Cattari S, Lagomarsino S, Giovinazzi S, Ingham JM, Marotta A, Liberatore D, Sorrentino L, Ottone D, Pinna M, et al. 2016. Vulnerability analysis of unreinforced masonry churches (EQC 14/660): final report. Lower Hutt (NZ): GNS Science. 132 p. Consultancy Report 2016/53. Prepared for: Earthquake Commission Research Foundation.
- Horspool NA, Chadwick MP, Ristau J, Salichon J, Gerstenberger MC. 2015. ShakeMapNZ: informing post-event decision making. In: *New dimensions in earthquake resilience: 2015 New Zealand Society for Earthquake Engineering Technical Conference and AGM*. 2015 Apr 10–12; Rotorua, New Zealand. Wellington (NZ): New Zealand Society for Earthquake Engineering.
- O'Rourke M, Deyoe E. 2004. Seismic damage to segmented buried pipe. *Earthquake Spectra*. 20(4):1167–1183. doi:10.1193/1.1808143.
- O'Rourke TD, Jeon SS. 1999. Factors affecting the earthquake damage of water distribution systems. In: Earthquake Engineering Research Institute, editor. *Proceedings, Sixth US National Conference on Earthquake Engineering*. 1998 May 31–Jun 4; Seattle, WA. Oakland (CA): Earthquake Engineering Research Institute. p. 379–388.
- O'Rourke TD, Jeon S-S, Toprak S, Cubrinovski M, Hughes M, van Ballegooij S, Bouziou D. 2014. Earthquake response of underground pipeline networks in Christchurch, NZ. *Earthquake Spectra*. 30(1):183–204. doi:10.1193/030413eqs062m.
- Rojahn C, Sharpe RL. 1985. Earthquake damage evaluation data for California. Redwood City (CA): Applied Technology Council. 492 p. Report ATC-13.
- [SCIRT] Stronger Christchurch Infrastructure Rebuild Team. 2013. Assessing assets to utilise remaining asset life and avoid repairing non-critical defects. Christchurch (NZ): Stronger Christchurch Infrastructure Rebuild Team.
- Smith WD. 2002. A model for MM intensities near large earthquakes. *Bulletin of the New Zealand National Society for Earthquake Engineering*. 35(2):96–107.
- Stirling MW, Gerstenberger MC, Goded T, Ries W. 2015. Macroseismic intensity assessment for the M6.2 2011 Christchurch earthquake. Lower Hutt (NZ): GNS Science. 51 p. Consultancy Report 2015/26. Prepared for: EQC.
- Tonkin & Taylor. 2013. Liquefaction vulnerability study. [Christchurch] (NZ): Tonkin & Taylor. Report 52020.0200/v1.0. Prepared for Earthquake Commission.
- van Ballegooij S, Malan P, Lacrosse V, Jacka ME, Cubrinovski M, Bray JD, O'Rourke TD, Crawford SA, Cowan H. 2014. Assessment of liquefaction-induced land damage for residential Christchurch. *Earthquake Spectra*. 30(1):31–55. doi:10.1193/031813eqs070m.
- Worden CB, Gerstenberger MC, Rhoades DA, Wald DJ. 2012. Probabilistic relationships between ground-motion parameters and modified Mercalli intensity in California. *Bulletin of the Seismological Society of America*. 102(1):204–221. doi:10.1785/0120110156.
- Zare MR. 2012. The effects of earthquakes on wastewater pipelines in New Zealand: evaluation and rehabilitation [PhD thesis]. Auckland (NZ): University of Auckland. 249 p.

This page left intentionally blank.

APPENDICES

This page left intentionally blank.

APPENDIX 1 MODIFIED MERCALLI SEISMIC INTENSITY SCALE FOR NEW ZEALAND

MM1 People

Not felt, except by a very few people under exceptionally favourable circumstances.

MM2 People

Felt by persons at rest, on upper floors or who are favourably placed.

MM3 People

Felt indoors; hanging objects may swing, vibration similar to passing of light trucks, duration may be estimated, may not be recognised as an earthquake.

MM4 People

Generally noticed indoors but not outside. Light sleepers may be awakened. Vibration may be likened to the passing of heavy traffic or to the jolt of a heavy object falling or striking the building.

Fittings

- Doors and windows rattle. Glassware and crockery rattle. Liquids in open vessels may be slightly disturbed. Standing motorcars may rock.

Structures

- Walls and frames of buildings, and partitions and suspended ceilings in commercial buildings, may be heard to creak.

MM5 People

- Generally felt outside, and by almost everyone indoors.
- Most sleepers awakened.
- A few people alarmed.

Fittings

- Small unstable objects are displaced or upset. Some glassware and crockery may be broken.
- Hanging pictures knock against the wall.
- Open doors may swing.
- Cupboard doors secured by magnetic catches may open.
- Pendulum clocks start, stop or change rate (H).

Structures

- Some Windows Type I cracked.
- A few earthenware toilet fixtures cracked (H).

MM6 People

- Felt by all.
- People and animals alarmed.
- Many run outside.
- Difficulty experienced in walking steadily.

Fittings

- Objects fall from shelves.
- Pictures fall from walls (H).
- Some furniture moved on smooth floors; some unsecured free-standing fireplaces moved.
- Glassware and crockery broken.
- Very unstable furniture overturned.
- Small church and school bells ring (H).
- Appliances move on bench or table tops.
- Filing cabinets or 'easy glide' drawers may open (or shut).

Structures

- Slight damage to Buildings Type I.
- Some stucco or cement plaster falls.
- Windows Type I broken.
- Damage to a few weak domestic chimneys; some may fall.

Environment

- Trees and bushes shake or are heard to rustle.
- Loose material dislodged on some slopes, e.g. existing slides, talus and scree slopes.
- A few very small ($\leq 10^3 \text{ m}^3$) soil and regolith slides and rock falls from steep banks and cuts.
- A few minor cases of liquefaction (sand boil) in highly susceptible alluvial and estuarine deposits.

MM7 People

- General alarm.
- Difficulty experienced in standing.
- Noticed by motorcar drivers who may stop.

Fittings

- Large bells ring.
- Furniture moves on smooth floors, may move on carpeted floors.
- Substantial damage to fragile contents of buildings.

Structures

- Unreinforced stone and brick walls cracked.
- Buildings Type I cracked; some with minor masonry falls.
- A few instances of damage to Buildings Type II.
- Unbraced parapets, unbraced brick gables and architectural ornaments fall.
- Roofing tiles, especially ridge tiles may be dislodged.
- Many unreinforced domestic chimneys damaged, often falling from roof line.
- Water tanks Type I burst.
- A few instances of damage to brick veneers and plaster or cement-based linings.
- Unrestrained water cylinders (Water Tanks Type II) may move and leak.
- Some Windows Type II cracked.
- Suspended ceilings damaged.

Environment

- Very small ($\leq 10^3 \text{ m}^3$) disrupted soil slides and falls of sand and gravel banks, and small rock-falls from steep slopes and cuttings are common.
- Fine cracking on some slopes and ridge crests.
- A few small to moderate landslides ($10^3\text{--}10^5 \text{ m}^3$), mainly rock falls on steeper slopes ($> 30^\circ$) such as gorges, coastal cliffs, road cuts and excavations.
- Small discontinuous areas of minor shallow sliding and mobilisation of scree slopes in places.
- A few instances of non-damaging liquefaction (small water and sand ejections) in alluvium.

MM8 People

- Alarm may approach panic.
- Steering of motorcars greatly affected.

Structures

- Buildings Type I heavily damaged; some collapse.
- Buildings Type II damaged, some with partial collapse.
- Buildings Type III damaged in some cases.
- A few instances of damage to Structures Type IV.
- Monuments and pre-1976 elevated tanks and factory stacks twisted or brought down.
- Some pre-1965 infill masonry panels damaged.
- A few post-1980 brick veneers damaged.
- Decayed timber piles of houses damaged.
- Houses not secured to foundations may move.
- Most unreinforced domestic chimneys damaged; some below roof-line; many brought down.

Environment

- Cracks appear on steep slopes and in wet ground.
- Significant landsliding likely in susceptible areas.
- Small to moderate slides (10^3 – 10^5 m 3) widespread; mainly rock and disrupted soil falls on steeper slopes (steep banks, terrace edges, gorges, cliffs, cuts, etc).
- Significant areas of shallow regolith landsliding, and some reactivation of scree slopes.
- A few large (10^5 – 10^6 m 3) landslides from coastal cliffs, and possibly large to very large ($\geq 10^6$ m 3) rock slides and avalanches from steep mountain slopes.
- Larger landslides in narrow valleys may form small temporary landslide-dammed lakes.
- Roads damaged and blocked by small to moderate failures of cuts and slumping of road-edge fills.
- Evidence of soil liquefaction common, with small sand boils and water ejections in alluvium, and localised lateral spreading (fissuring, sand and water ejections) and settlements along banks of rivers, lakes and canals, etc.

MM9 Structures

- Many Buildings Type I destroyed.
- Buildings Type II heavily damaged; some collapse.
- Buildings Type III damaged, some with partial collapse.
- Structures Type IV damaged in some cases; some with flexible frames seriously damaged.
- Damage or permanent damage to some Structures Type V.
- Houses not secured to foundations shifted off.
- Brick veneers fall and expose frames.

Environment

- Cracking on flat and sloping ground conspicuous.
- Landsliding widespread and damaging in susceptible terrain, particularly on slopes steeper than 20°.
- Extensive areas of shallow regolith failures and many rock falls and disrupted rock and soil slides on moderate to steep slopes (20°–35° or greater), cliffs, escarpments, gorges and man-made cuts.
- Many small to large (10^3 – 10^6 m 3) failures of regolith and bedrock, and some very large landslides ($\geq 10^6$ m 3) on steep susceptible slopes.
- Very large failures on coastal cliffs and low-angle bedding planes in Tertiary rocks. Large rock/debris avalanches on steep mountain slopes in well-jointed greywacke and granitic rocks. Landslide-dammed lakes formed by large landslides in narrow valleys.
- Damage to road and rail infrastructure widespread with moderate to large failures of road cuts and slumping of road-edge fills. Small to large cut slope failures and rock falls in open mines and quarries.
- Liquefaction effects widespread, with numerous sand boils and water ejections on alluvial plains, and extensive, potentially damaging lateral spreading (fissuring and sand ejections) along banks of rivers, lakes, canals, etc. Spreading and settlement of river stopbanks likely.

MM10 Structures

- Most Buildings Type I destroyed.
- Many Buildings Type II destroyed.
- Many Buildings Type III heavily damaged; some collapse.
- Structures Type IV damaged, some with partial collapse.
- Structures Type V moderately damaged, but few partial collapses.
- A few instances of damage to Structures Type VI.
- Some well-built timber buildings moderately damaged (excluding damage from falling chimneys).

Environment

- Landsliding very widespread in susceptible terrain.
- Similar effects to MM9, but more intensive and severe, with very large rock masses displaced on steep mountain slopes and coastal cliffs. Landslide-dammed lakes formed. Many moderate to large failures of road and rail cuts and slumping of road-edge fills and embankments may cause great damage and closure of roads and railway lines.
- Liquefaction effects (as for MM9) widespread and severe. Lateral spreading and slumping may cause rents over large areas, causing extensive damage, particularly along river banks, and affecting bridges, wharves, port facilities, and road and rail embankments on swampy, alluvial or estuarine areas.

MM11 Structures

- Most Buildings Type II destroyed.
- Many Buildings Type III destroyed.
- Structures Type IV heavily damaged; some collapse.
- Structures Type V damaged, some with partial collapse.
- Structures Type VI suffer minor damage, a few moderately damaged.

MM12 Structures

- Most Buildings Type III destroyed.
- Many Structures Type IV destroyed.
- Many Buildings Type V heavily damaged, some with partial collapse.
- Structures Type VI moderately damaged.

Categories of Construction

Buildings Type I:

Buildings with a low standard of workmanship, poor mortar, or that are constructed of weak materials like mud brick or rammed earth. Soft storey structures (e.g. shops) made of masonry, weak reinforced concrete or composite materials (e.g. some walls timber, some brick) not well tied together. Masonry buildings otherwise conforming to Buildings Types I–III, but also having heavy unreinforced masonry towers. (Buildings constructed entirely of timber must be of extremely low quality to be Type I).

Buildings Type II:

Buildings of ordinary workmanship, with mortar of average quality. No extreme weaknesses, such as inadequate bonding of the corners, but neither designed nor reinforced to resist lateral forces. Such buildings not having heavy unreinforced masonry towers.

Buildings Type III:

Reinforced masonry or concrete buildings of good workmanship and with sound mortar, but not formally designed to resist earthquake forces.

Structures Type IV:

Buildings and bridges designed and built to resist earthquakes to normal use standards, i.e. no special collapse or damage limiting measures taken (mid-1930s to c. 1970 for concrete and to c.1980 for other materials).

Structures Type V:

Buildings and bridges designed and built to normal use standards, i.e. no special damage limiting measures taken, other than code requirements, dating from c. 1970 for concrete and c.1980 for other materials.

Structures Type VI:

Structures, dating from c. 1980, with well-defined foundation behaviour, which have been specially designed for minimal damage, e.g. seismically isolated emergency facilities, some structures with dangerous or high contents, or new generation low-damage structures.

Windows Type I:

Large display windows, especially shop windows.

Windows Type II:

Ordinary sash or casement windows.

Water Tanks Type I:

External, stand-mounted, corrugated iron water tanks.

Water Tanks Type II:

Domestic hot-water cylinders unrestrained except by supply and delivery pipes.

H (Historical):

Important for historical events. Current application only to older houses, etc.

General Comment:

- ‘Some’ or ‘a few’ indicates that the threshold of a particular effect has just been reached at that intensity.
- ‘Many run outside’ (MM6) variable depending on mass behaviour, or conditioning by occurrence or absence of previous quakes, i.e. may occur at MM5 or not until MM7.
- ‘Fragile contents of buildings’ – fragile contents include weak, brittle, unstable, unrestrained objects in any kind of building.
- ‘Well-built timber buildings’ have: wall openings not too large, robust piles or reinforced concrete strip foundations, superstructure tied to foundations.
- Buildings Type III–V at MM10 and greater intensities are more likely to exhibit the damage levels indicated for low-rise buildings on firm or stiff ground and for high-rise buildings on soft ground. By inference, lesser damage to low-rise buildings on soft ground and high-rise buildings on firm or stiff ground may indicate the same intensity. These effects are due to attenuation of short period vibrations and amplification of longer period vibrations in soft soils.

References

- Dowrick DJ. 1996. The modified Mercalli earthquake intensity scale ; revisions arising from recent studies of New Zealand earthquakes. *Bulletin of the New Zealand National Society for Earthquake Engineering*. 29(2):92–106.
- Hancox GT, Perrin ND, Dellow GD. 2002. Recent studies of historical earthquake-induced landsliding, ground damage, and MM intensity in New Zealand. *Bulletin of the New Zealand Society for Earthquake Engineering*. 35(2):59–95.
- [NZSEE] New Zealand Society for Earthquake Engineering. 1992. A revision of the modified Mercalli seismic intensity scale: Report of a study group of the NZSEE. *Bulletin of the New Zealand National Society for Earthquake Engineering*. 25(4):345–357.